

AMERICAN UNIVERSITY OF BEIRUT

FOCUSED ULTRASOUND NEUROMODULATION (FUS)
FOR PROLONGED SUPPRESSION OF PAIN RELATED
POTENTIALS

by
PETRA HASSAN RAAD

A thesis
submitted in partial fulfillment of the requirements
for the degree of Master of Engineering
to the Department of Mechanical Engineering
of Maroun Semaan Faculty of Engineering and Architecture
at the American University of Beirut

Beirut, Lebanon
September 2022

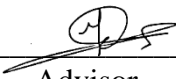
AMERICAN UNIVERSITY OF BEIRUT

FOCUSED ULTRASOUND NEUROMODULATION (FUS)
FOR PROLONGED SUPPRESSION OF PAIN RELATED
POTENTIALS


by
PETRA HASSAN RAAD

Approved by:

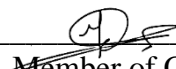
Dr. Massoud Khraiche, Assistant Professor
Department of Biomedical Engineering


Advisor

Dr. Kamel Ghali, Professor
Department of Mechanical Engineering


Member of Committee

Dr. Mohammad Harb, Assistant Professor
Department of Mechanical Engineering


Member of Committee

Dr. Nada Lawand, Assistant Professor
Department of Neurology


Member of Committee

Date of thesis defense: September 5, 2022

ACKNOWLEDGEMENTS

I would like to thank every entity who contributed to the making of the content of the thesis and the library staff who made the thesis available to readers.

I would also like to thank my brother Ragheb Raad, my mom Zanoubia Krayem, and my dad whose first name and last name are written immediately after my first name on the cover page.

I dedicate this work to first-generation students doing their master's degrees (especially female students). I also dedicate it to my late grandfathers and the former member of the board of trustees at AUB, Ali Ghandour. Ghandour died in August 2020 and was not able to attend the undergraduate commencement ceremony of class of 2020 that was postponed from June 2020 to October 2021. Finally, I dedicate this thesis to the revered person whose presence is similar to the sun hidden behind the clouds.

ABSTRACT OF THE THESIS OF

Petra Hassan Raad

for

Master of Engineering

Major: Mechanical Engineering

Title: Focused Ultrasound Neuromodulation (FUS) for Prolonged Suppression of Pain Related Potentials

Chronic pain has a major impact on quality of life. Treatment options for chronic pain include device-based electrical stimulation or pharmaceutical solutions. The challenges of these treatment options include safety of long-term application or patient addiction (to opioids-based drug therapies). Focused ultrasound (FUS) waves have emerged as a promising therapeutic tool for non-invasive neuromodulation of the central and peripheral nervous system. In this work, we investigated, through high-resolution acoustic imaging and custom designed phantoms, the attenuation effect of various skin layers on acoustic intensity and spatial resolution for noninvasive modulation of peripheral nerves. We also investigated, for the first time, the prolonged effect of noninvasive low-frequency low-intensity ultrasound in suppression of pain-evoked potentials in the reflex arc neural pathway in anesthetized animal. The experiments included applying US to electrically stimulated rat sciatic nerve (simulating pain potentials) at increasing sonication time (30, 60, 90 secs) and at varying duty cycle (31.25, 50, and 80 percent) and measuring resulting pain potentials through Electromyography (EMG) recordings. We found that increasing sonication time and duty cycle enhanced the prolonged suppression of pain related potentials. The US treatment also caused a shift in the median of the frequency components in the power spectrum of the EMG measurements. This indicates activation of new muscle fibers, possibly to compensate for activity suppression brought on by the US. This is interesting given we still observed a drop in both area under the curve (AUC) and amplitude of EMG. Overall, the study shows the potential to tune the prolonged suppressive effect of US on pain potentials, sheds light on potential changes in muscle fiber activation due to US and paves the way for potential applications of US in device-based treatment of chronic pain.

TABLE OF CONTENTS

ACKNOWLEDGEMENTS	1
ABSTRACT	2
ILLUSTRATIONS	6
TABLES	10
ABBREVIATIONS	11
INTRODUCTION	13
LITERATURE REVIEW	15
A. Current Pain Management or Treatment Solutions	15
1. Pharmacological Treatment (opioids and non-opioid Analgesics).....	15
2. Neuromodulation for Pain Treatment	16
B. Mechanisms by which FUS Alleviates Pain.....	18
1. FUS stimulation	19
2. FUS lesioning	20
3. Drug delivery via blood-brain barrier disruption.....	20
C. Use of FUS in Preclinical and Clinical Pain-related Studies.....	21
1. LIFUS to treat rabbits with soft tissue injury	21
2. FUS to treat patients with painful neuralgia or metastases.....	21
D. Lasting Effects of US-stimulation	23

INVESTIGATING CHANGE IN ACOUSTIC INTENSITY WITH REPSPECT TO US PARAMETERS	26
A. Experimental Setup and Procedure.....	27
B. Results and Discussion	29
1. effect of changing the DC by changing the BP	29
2. effect of raising the FF.....	31
3. effect of raising the input voltage that the function generator provides	31
4. effect of altering the medium properties.....	32
5. Similarities between tissues covering the sciatic nerve and gelatin phantom	40
 INVESTIGATING THE PROLONGED (OR OFFLINE) EFFECT OF LIFUS TARGETING THE SCAITIC NERVE OF ANESTHETIZED RATS	 41
A. Materials and Methods.....	41
1. Animals.....	41
2. Animal preparation	41
3. Ultrasound parameters	43
4. Experimental procedure.....	44
5. EMG data analysis	46
B. Results.....	47
C. Discussion.....	52
1. Potential of LIFUS in inducing prolonged change in neural activity	52
2. Possible mechanisms through which sonication modulated muscle activity .	54
 CONCLUSION AND FUTURE WORK.....	 65
 APPENDIX	 66

A. Calculation of Acoustic Intensity.....	66
B. Properties of devices used in experiments of Chapter III	68
C. Full-width colormaps	70
D. Preparation of the gelatin-based phantom (section B.3 of Chapter II)	73
E. Time plots of amplitude and AUC for each trial (experiments of chapter IV)	74
F. The processes that lead to movement of skeletal muscle	76
G. Structures of ion channels	77
REFERENCES	79

ILLUSTRATIONS

Figure

1.	3D cross sectional view of ultrasound stimulation (Joe et al., 2019)	13
2.	Physical neuromodulation technologies. a) A diagram illustration for spinal cord stimulation (SCS). b) invasive techniques: including deep brain stimulation (DBS) and motor cortical stimulation (MCS). c) noninvasive modalities: transcranial current stimulation (TCS), transcranial magnetic stimulation (TMS), and transcranial focused ultrasound stimulation (tFUS) (Yu et al., 2020).	16
3.	Schematic overview of FUS treatments for neurological conditions including chronic pain (M. Zhang et al., 2022)	19
4.	Definition of sonication parameters: inter-stimulus interval (ISI), sonication duration (SD), tone-burst duration (TBD), duty cycle (DC), and pulse-repetition period (PRP) (Dell'Italia et al., 2022). The signal propagates at a fundamental frequency (FF). Note: $TBD = CPP / FF$, and $BP = PRP$, where CPP= number of cycles per pulse, and BP= burst period. The BP represents the time interval separating each burst in pulsed signal. The DC represents the portion of the BP in which the amplitude of the signal is non zero. The PRF represents the number of pulses generated per second for a pulsed signal.	26
5.	Schematic Diagram of Acoustic Profile Setup (edited from El Hassan, 2020)..	27
6.	the profile of the normalized spatial-peak pulse average intensity (I_{SPPA}) for $FF = 1$ MHz at different DCs. (Max= approximately 3 W/cm^2). The red arrow indicates the direction of US waves. The Onda HNR-0500 hydrophone measured the voltage in the experiments of this subsection. A full-width version of each colormap of figure 6 is provided in Appendix C.	30
7.	Plot of intensity function of longitudinal distance for input voltage amplitudes of 75 mVpp (blue curve with asterix markers), 150 mVpp (red curve with square markers), and 225 mVpp (grey curve with 'x' markers). The arrow next to the bottom axis represents the direction of US waves. ($FF = 1$ MHz, DC= 50 percent). The Sonic Concepts Y-104-023 captured the voltages in the experiments of this subsection.	32
8.	refrigerated gelatin inserted in a frame and positioned in front of the US source.	34
9.	Plot of spatial-peak pulse-average intensity function of concentration. The error bar corresponds to one standard deviation. A zero concentration corresponds to propagation in water.	35
10.	Plot of attenuation coefficient of gelatin-based tissue mimicking phantom function of gelatin concentration. The error bar represents one standard deviation.	35

11. colormaps of normalized I_{SPPA} for each gelatin concentration where the shades of color correspond to the ratio of the local intensity with respect to I_{SPPA} in water (without phantom). Maximum local intensities are 0.70 W/cm^2 in water, 0.62 W/cm^2 with 12.5 percent gelatin phantom, 0.58 W/cm^2 with 20 percent gelatin, and 0.30 W/cm^2 with 24 percent gelatin.	36
12. colormap of of normalized I_{SPPA} where the shades of color correspond to the ratio of the local intensity with respect to I_{SPPA} in water (without phantom). Maximum intensities are 0.65 W/cm^2 in water, and 0.50 W/cm^2 with 12.5 percent gelatin phantom. The arrow indicates the direction of US waves. In the side view map, the direction of US in into the page.	37
13. plot of Young’s modulus of the gelatin-based tissue mimicking phantom function of gelatin concentration. The error bar represents one standard deviation.....	38
14. Stress-strain curve of three gelatin-based tissue mimicking phantom specimen with concentrations of 12.5, 20 and 24 percent. Displacement rate= 0.1 mm/s . Stopping condition: maximum strain of 0.4 mm/mm	39
15. Photo of experimental setup. The stimulating electrode is hooked to the exposed sciatic nerve. The transducer is coupled with cone filled with ultrasound gel that serves as a medium for propagation.	42
16. schematic of the animal experiment (components of figure extracted from Coutinho et al., 2020 and Liu et al., 2021). (1) function generator. (2) amplifier. (3) oscilloscope. (4) transducer targeting the exposed sciatic nerve. (5) stimulating electrode hooked to nerve. (6) EMG electrode inserted in gastrocnemius muscle.	42
17. Experimental procedure. The electrical stimulation parameters are: amplitude= 5 volts, frequency= 2 Hz, duration of pulse= 2 ms, and delay = zero ms.	45
18. sample plots of stimulus, signal emitted by the generator before being converted to US, and amplified EMG.	46
19. Region A corresponds to initial 30-second interval before onset of treatment. Region B is the last 30 seconds of the sonication duration where the nerve received both electrical stimulation and US treatment. Region D is the last 30-second interval in the trial before stopping EMG recording.	47
20. average percentage change in amplitude and AUC as function of DC, where percentage change is $=100*(\text{value in region D in current trial} - \text{value in region A in current trial})/\text{value in region A in current trial}$. The error bar represents one standard deviation.	48
21. average percentage change in amplitude and AUC as function of $I_{SPTA} * SD$ for the same trial. The error bar represents one standard deviation.	49
22. average percentage change in amplitude and AUC as function of DC, where percentage change is $=100*(\text{value in region A in trial after} - \text{value in region D$	

in current trial)/value in region D in current trial. The error bar represents one standard deviation.	50
23. average percentage change in amplitude and AUC as function of $I_{SPTA} * SD$ compared across trials on the same rat. The error bar represents one standard deviation.....	50
24. Median Frequency for each trial. One error bar represents one standard deviation. Credits: Heba Badawe.....	51
25. Stress-strain relationship for (a) an ideal elastic, (b) for viscoelastic matter (b) (Azhari, 2010, p. 96), and (c) for the sciatic nerve samples of Chen et al. (2010b) under cyclic loading.....	58
26. Zener model representing the viscoelastic material as (a) a spring in series with a Kelvin model, and (b) a spring in parallel with a Maxwell model (McCrum et al., 2001, p. 141). J_R and J_U are the time-independent compliances. $[\eta]$ is the damper coefficient. ($J_d = J_R - J_U$ is the time-dependent compliance). G is the stress relaxation modulus.....	59
27. vector representation of an alternating stress leading a strain by a phase angle δ (McCrum et al., 2001, p. 129) at steady state. $[\omega]$ is the angular frequency. $[\sigma]$ is oscillatory stress. $[\gamma]$ is the oscillatory strain.....	60
28. reaction force of prostate specimen receiving uniaxial sinusoidal force (Palacio-Torralba et al., 2015). The reaction force starts with a transient response.	61
29. exponential decay of the strain of a viscoelastic material. The time constant varies from 60 seconds to 210 seconds.....	62
30. Colormap of normalized spatial-peak pulse average intensity (I_{SPPA}) at FF= 1 MHz. DC= 31.25 percent. The black double arrow represents the diameter of the focus measured at FWHM (4 mm). The red arrow indicates the direction of US. (Parameters: FF= 1 MHz. CPP=250. BP= 800 μ s. Amplitude of generated signal= 225 mVpp.)	70
31. Colormap of normalized spatial-peak pulse average intensity (I_{SPPA}) at FF= 1 MHz. DC= 50 percent. The black double arrow represents the diameter of the focus measured at FWHM (4 mm). The red arrow indicates the direction of US. (Parameters: FF= 1 MHz. CPP=250. BP= 500 μ s. Amplitude of generated signal= 225 mVpp.)	71
32. Colormap of normalized spatial-peak pulse average intensity (I_{SPPA}) at FF= 1 MHz. DC= 31.25 percent. The black double arrow represents the diameter of the focus measured at FWHM (4 mm). The red arrow indicates the direction of US. (Parameters: FF= 1 MHz. CPP=250. BP= 312.5 μ s. Amplitude of generated signal= 225 mVpp.)	72
33. Trials of August 16 and 17. Mean amplitude with a polynomial fit. The bars correspond to start and end of sonication session.....	74

34. Trials of August 16 and 17. Mean AUC computed for each 15-second interval in each trial along with a polynomial fit. The bars correspond to start and end of sonication session.	75
35. Trials of August 25. Mean amplitude with a polynomial fit. The shaded area represents sonication session. The points on the limits of the shaded area belong to the area.....	76
36. Trials of August 25. Mean AUC with a polynomial fit. The shaded area represents sonication session. The points on the limits of the shaded area belong to the area.....	76
37. structure of the VGKCs of the Kv subfamily (Gamper & Wang, 2021, p. 6). The channel has a voltage-sensing domain (VSD) that detects voltage difference during firing, and a pore domain through which potassium ions diffuse.	77
38. (a) schematic of overall structure of voltage-gated sodium channel (Nav), having a VSD, and a pore domain. (b) Top view of overall model of eukaryotic (left) and bacterial (right) voltage-gated sodium channel (Chahine, 2018, p.55).....	78

TABLES

Table

1. sets of experimental parameters that explore effect of DC on intensity	29
2. summary of the results of acoustic profile experiments.	31
3. set of experimental parameters where US targets the sciatic nerve. A DC of 100 percent represents a continuous pulse. FF= 500 kHz. CPP= 125. TBD= 250 microsecond. Amplitude of signal at function generator output= 180 mVpp. ...	44
4. time-dependent moduli and relaxation time constants of animal tissues.....	63
5. Properties of Olympus focused transducers used in the experiments of Chapter III	68
6. EOC sensitivity and capacitance of the Sonic Concepts Y-104-023 hydrophone used in experiments of subsection B.3. of Chapter III.....	69
7. EOC sensitivity and capacitance of the Onda HNR-0500 hydrophone used in experiments of subsection B.1, B.2, and B.4 of Chapter III.....	69

ABBREVIATIONS

ACh	Acetylcholine
ARF	Acoustic radiation force
AUC	Area under the curve
BBB	Blood-brain barrier
BP	Burst period
CDC	Centers for Disease Control and Prevention
CLT	Central lateral thalamotomy
CPP	Cycles per pulse
DBS	Deep brain stimulation
DC	Duty cycle
EMG	Electromyogram
EOC	End-of-cable
FF	Fundamental frequency
FUS	Focused ultrasound
FWHM	Full-width at half maximum
IPG	Implantable pulse generator
I _{SPPA}	Spatial-peak pulse-average intensity
I _{SPTA}	Spatial-peak temporal-average intensity
LIFUS	Low-intensity FUS
MCS	Motor cortex stimulation
MRgFUS	Magnetic resonance-guided FUS
NSAIDS	Non-steroid anti-inflammatory drugs

PAG	Periaqueductal gray
PD	Pulse duration
PII	Pulse Intensity Integral
PRF	Pulse-repetition frequency
PVG	Periventricular gray matter
SCS	Spinal cord stimulation
STI	Soft tissue injury
TBD	Tone-burst duration
tDCS	Transcranial direct current stimulation
TCS	Transcranial current stimulation
tFUS	Transcranial FUS
TMS	Transcranial magnetic stimulation
TN	Trigeminal neuralgia
USgFUS	Ultrasound-guided FUS
VGKC	Voltage-gated potassium channel
VSD	Voltage-sensing domain

CHAPTER I

INTRODUCTION

Chronic pain is defined as persistent or recurrent pain lasting longer than 3 months (Todd et al., 2020). It is the result of abnormalities in function, structure, or chemistry within the nervous system. Pharmacological methods are the most common treatment option due to cost and ease of use. However, pharmacological drugs lead to severe side effects such as addiction, overdose, and death (Yu et al., 2020).

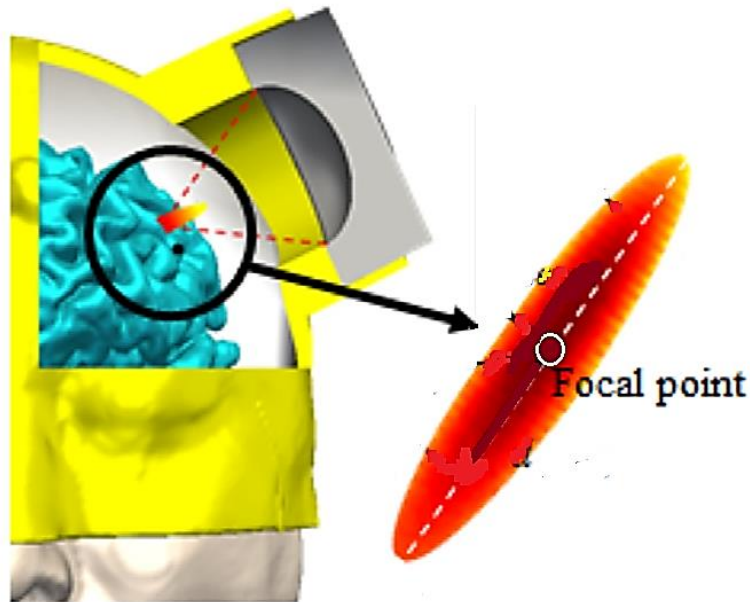


Figure 1: 3D cross sectional view of ultrasound stimulation (Joe et al., 2019)

To overcome the side effects of drugs, neuromodulation techniques are employed, where neuromodulation is the use of electrical or chemical stimuli to modify the activity of nervous system with therapeutical purposes (da Silva Freitas et al., 2022, p. 1).

One of the emerging noninvasive neuromodulation techniques for pain treatment is focused ultrasound (FUS) where a transducer is positioned above the targeted area. The transducer will emit focused ultrasonic waves that transfer energy when propagating (figure 1). The ultrasound energy converges at one location, called the focus or focal point, to create an amplified effect without affecting the regions surrounding the target (Todd et al., 2020).

In the upcoming chapters, we first elaborate on the limitations of the current pain treatment methods, then discuss studies in which FUS successfully modulated pain sensation. After that, we investigate the use of low-intensity focused ultrasound (LIFUS) in alleviating pain by targeting the sciatic nerve of anesthetized rats. The investigation starts by studying how the intensity of FUS changes when modifying the experimental parameters such as frequency, burst period and the medium of propagation. After exploring the change of intensity as function of parameters, we discuss the results of the experiments on rodents whose aim was to determine the prolonged effect (or offline effect) of LIFUS in the treatment of chronic pain. In these preclinical studies, anesthetized rats have their sciatic nerve exposed, electrically stimulated, and treated with US waves.

CHAPTER II

LITERATURE REVIEW

A. Current Pain Management or Treatment Solutions

1. Pharmacological Treatment (opioids and non-opioid Analgesics)

Analgesic medications, such as opioids, are cheap and routinely prescribed for acute pain (Yu et al., 2020). However, their consumption has become a public health concern. The Centers for Disease Controls and Prevention (CDC) in the United States declared in 2012 the overuse of opioids and opioid-related deaths an epidemic (CDC, 2012). In the United Kingdom, the number of opioid-related mortalities per one million inhabitants went up by 56.6 percent between 2010 and 2018 (Kurdi, 2021).

Strong opioids (such as morphine and oxycodone) were found to be more efficient than non-opioid drugs, whereas weak opioids (such as tramadol and codeine) were of the same efficiency in pain reduction compared to non-steroid anti-inflammatory drugs (NSAIDS). In addition, it was found that each individual responds differently to opioids (Kalso et al., 2004), and that their use leads paradoxically to sensitivity to pain (Kohno et al., 2005). Thus, NSAIDs are used to avoid the adverse events of opioids.

These drugs reduce inflammation or the production of inflammatory factors to reduce pain sensation. However, chronic consumption of NSAIDS at high doses harms the kidneys and the stomach. Populations with history of cardiovascular diseases and stroke are also recommended to avoid using NSAIDS (Yu et al., 2020). Hence, pharmacological treatment of pain is limited by the adverse events of drugs and their inconsistent responsiveness.

2. Neuromodulation for Pain Treatment

Neuromodulation techniques modify the activity of the central and peripheral nervous system by delivering electrical, magnetic, or mechanical energy to the patient's anatomy (Yu et al., 2020). These techniques, illustrated in figure 1, can be excitatory or inhibitory, invasive, or non-invasive. Invasive techniques include spinal cord stimulation (SCS), motor cortex stimulation (MCS), and deep brain stimulation (DBS). Whereas non-invasive techniques include transcranial magnetic stimulation (TMS), transcranial current stimulation (TCS), and transcranial focused ultrasound (tFUS). Invasive techniques are considered after pharmacological treatment have been deemed inefficient or addictive.

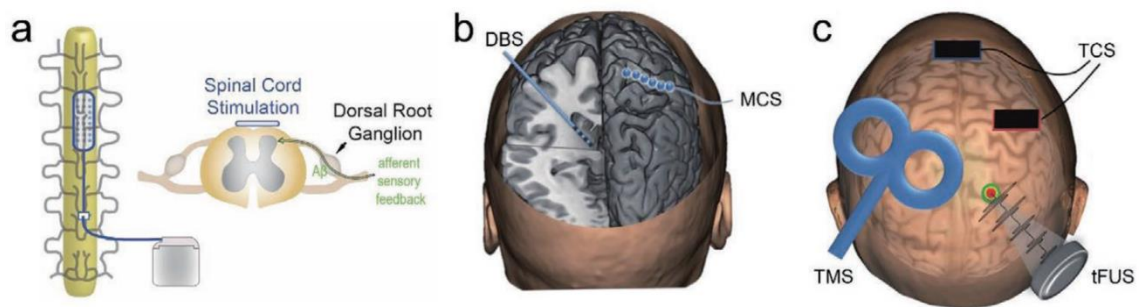


Figure 2: Physical neuromodulation technologies. a) A diagram illustration for spinal cord stimulation (SCS). b) invasive techniques: including deep brain stimulation (DBS) and motor cortical stimulation (MCS). c) noninvasive modalities: transcranial current stimulation (TCS), transcranial magnetic stimulation (TMS), and transcranial focused ultrasound stimulation (tFUS) (Yu et al., 2020).

a. Invasive Neuromodulation (SCS, MCS, and DBS)

SCS inhibits the spinal cord signaling in the central nervous system. Electrodes are implanted subdermally to deliver electric signals to the dorsal horn and dorsal column axons (figure 2.a), which hinders pain signaling in the spinothalamic tract.

However, the efficacy of SCS in pain reduction decays in the long run as a result of the encapsulation of the electrodes as a foreign body response (Shamji et al., 2017).

MCS has been shown to alleviate pain caused by multiple sclerosis (Tanei et al., 2010), phantom limb pain (Roux et al., 2001), and spinal cord injury (Nguyen et al., 1999). Following localized craniotomies, epidural stimulation electrodes are placed on the motor cortex (figure 2.b); stimulation frequencies are in the range of 50 Hz. The use of MCS is limited by the difficulty to determine patient population that will respond to treatment, especially given its invasiveness (Yu et al., 2020).

DBS involves planting electrodes into deep brain (figure 2.b). The electrodes can target the sensory thalamus lateral and medial nuclei, internal capsule, and periaqueductal-periventricular gray matter (PAG-PVG). The components of DBS include thin lead implanted at the targeted area, an implantable pulse generator (IPG), wires connecting the lead to the IPG, and a patient programmer that allows physicians to connect with the IPG wirelessly, via radio frequency or Bluetooth, to adjust the stimulation parameters (Yu et al., 2020). Despite its high specificity, DBS has adverse events related to implantation (such as infection risks), hardware failure (such as IPG material erosion), and stimulation induced damage.

b. Noninvasive Neuromodulation (TMS, TCS, and tFUS)

TMS uses a coil of wire to generate rapidly changing magnetic fields (figure 2.c), which causes electromagnetic induction and eddy currents within the brain that alter brain activities. TMS is limited by its focality and penetration depth. The choice of material and design of the TMS coil also affects the efficacy of the treatment, the delivery of charge to the tissue, focality of induced electric fields, and depth of electric

penetration. In addition, TMS is limited by potential discomfort at the stimulation site and headache (Yu et al., 2020).

TCS uses rectangular or ring electrodes attached to the scalp that send low levels of current to modulate cortical excitability (figure 2.c) (Priori et al., 1998). Like TMS, TCS is limited by focality, penetration depth, and potential discomfort. Potential safety hazards also constraint the amount of current that can be delivered.

Unlike TMS and TCS, tFUS applied at low intensity can change neural activity with high spatial resolution, adjustable focus, and relatively low tissue attenuation (Yu et al., 2020). During tFUS neuromodulation, a transducer emits ultrasonic waves which will transfer highly pulsed and controllable mechanical energy when propagating through the skull (figure 2.c). The result is either activation or inhibition of neural activity according to the parameters. To reduce pain sensation, tFUS should induce inhibitory effects in the brain areas involved in perception of pain or excite circuits that suppress downstream brain functions (Bobola et al., 2018).

B. Mechanisms by which FUS Alleviates Pain

Todd et al. (2020) provided in their review an in-depth look at the application of FUS with emphasis on its use in treatments of chronic pain in the central nervous system (CNS), where chronic pain is defined as a persistent or recurrent pain lasting longer than 3 months. Ultrasound parameters can be varied to achieve one of the following mechanisms to reduce pain sensation: inhibition/stimulation of neuronal activity, thermal ablation of the tissue, or temporary disruption of the blood-brain barrier (BBB) (figure 3). According to the authors, irregular activity within, and connection between brain regions collectively gives rise to the experience of pain. FUS

selectively targets any of the pain network nodes to bring the brain activity back to the pre-pain state.

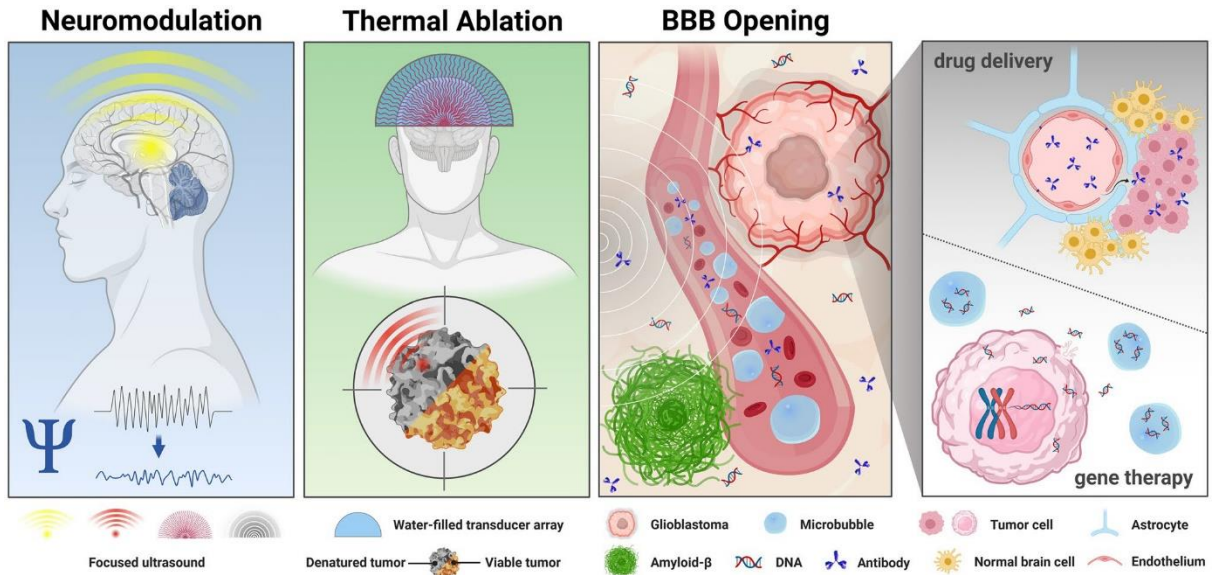


Figure 3: Schematic overview of FUS treatments for neurological conditions including chronic pain (M. Zhang et al., 2022)

1. *FUS stimulation*

Modulation of neural activity is achieved by applying the FUS in repeated bursts but at lower power. The direct action of the mechanical forces on cells causes the modulation of neuronal activity, either excitation or suppression, depending on the parameters used. Ultrasound exerts a mechanical force on the lipid bilayer of cell membranes. Several authors modelled the biophysics of the interaction to understand the mechanism by which US alters the electrical activity of neuronal cells (Krasovitski et al., 2011; Naor et al., 2016; Plaksin et al., 2016).

These models predict that the mechanical energy that the US delivers is converted to oscillations of the intramembrane space which could lead to neuronal excitation or inhibition, changes to membrane's capacitance which could drive a

current, opening of pores in the membrane lipid bilayer which would allow ions to flow, or activation of mechanosensitive ion channels (Blackmore et al., 2019).

2. *FUS lesioning*

Ablation or lesioning of the tissue is achieved by applying continuously the ultrasound at high power where the tissue is heated to above 60 °C under 30 seconds (Todd et al, 2020). One limitation of ablative treatment using FUS is the tradeoff in heating at the focus (the target) versus heating at the skull surface. As the target moves closer to the skull, the ratio of skull-to-focus surface areas decreases. The skull and focus receive the same amount of energy, but the former has a smaller area thus it is heated more than the focus. Another limitation is treating large volumes of tissue. Researchers are aiming at overcoming the mentioned challenges.

3. *Drug delivery via blood-brain barrier disruption*

Temporary disruption of the BBB is achieved by combining FUS with circulating microbubbles. The latter enter in a state of stable cavitation in the blood vessel as a result of the ultrasonic waves. The vibrations then disrupt the tight junctions that make the BBB. Hence, normally-non-penetrant agents become able to access the barrier (Todd et al., 2020). Similarly to ablation, opening larger volumes is also a challenge. Another concern is the shock waves that the microbubbles produce, violent enough to damage the tissue. On the other hand, heating is not a concern.

C. Use of FUS in Preclinical and Clinical Pain-related Studies

Several researchers explored the use of FUS in alleviating pain caused either by an injury or a disease.

1. LIFUS to treat rabbits with soft tissue injury

Liang et al. (2020) investigated the mechanism of LIFUS used in relieving pain caused by soft tissue injury (STI). In their experiments, 60 rabbits were lightly anesthetized, and their shaved left hind leg received three hammer blows on the thigh muscle to form an STI. The rabbits were separated into two groups: a group of 30 rabbits receiving LIFUS treatment daily for 10 consecutive days, and a group of 30 rabbits not receiving treatment (called control group). A transducer that emits LIFUS was pressed against the injured region. The concentrations of beta-endorphin were measured.

The authors explained that the LIFUS-treated rabbits had higher beta-endorphin levels in their blood than the control group. This result suggests that LIFUS stimulates the neurons to release the molecules that play a vital analgesic role. Regarding the effect of ultrasound on inflammation, the LIFUS treatment decreased the expression of inflammatory factors compared to untreated injured rabbits, without damaging the skin or intestines, usually harmed by anti-inflammatory drugs.

2. FUS to treat patients with painful neuralgia or metastases

As for clinical pain-related studies, Gallay et al. (2020) analyzed the use of bilateral magnetic-resonance-guided focused ultrasound central lateral thalamotomy (MRgFUS CLT) in treating trigeminal neuralgia (TN, chronic pain in trigeminal nerve).

Eight patients with chronic therapy-resistant TN were treated and followed up for a mean period of 53 months (range 12-92 months). The patients were requested to assess the percentage of postoperative pain relief relatively to preoperative pain.

Three months following the treatment, patients assessed a 51 percent mean pain relief, a 71 percent mean at 1 year, and a 78 percent mean at the longest follow-up. Five patients showed pain paroxysms at last follow-up, but their mean intensity decreased significantly following the operation. The scoring of the Mean Anxiety and Depression Scale also went down following operation. No serious adverse events occurred post operation. Thus, the use of MRgFUS CLT to treat eight patients with trigeminal pain, followed-up over 4 years, showed that the intervention is not risky and relieved the patients from pain significantly. The authors recommended experimenting on a larger sample size.

Drost et al. (2020) made another clinical study where they used ultrasound-guided FUS (USgFUS) to treat nine patients with painful bone metastases, instead of MRgFUS. The aim of the study was to evaluate the safety of USgFUS and its contribution in pain reduction and quality of life. The USgFUS device was positioned over the treatment area. The patients underwent a ten-day follow-up where the safety and efficacy of the procedure were evaluated daily. The patients were requested to report any adverse events following the procedure. The quality of life and pain were also assessed.

All patients except two experienced a decrease in pain by the tenth day. The average pain score of the patients fell from 6.9 prior the sonication sessions, to 3.2 on the tenth day (on a scale of zero to ten). Consumption of pain relievers also dropped. In

addition, the quality of life of the patients was improved, based on the answers which the patients provided to do the assessment.

The use of USgFUS in treating bone metastases was safe, tolerable, and beneficial in reducing pain and improving quality of life. The obtained results were consistent with previous studies that employed MRgFUS in the treatment of painful bone metastases. However, USgFUS was less painful, produced less adverse events, and did not require general anesthesia. The authors treated in their pilot study smaller targets because safety was the primary concern. The study had several limitations: a relatively short follow-up time of ten days, a small sample size, and considerable caution when treating patients.

D. Lasting Effects of US-stimulation

The extent to which the neuromodulatory effects of ultrasound are sustained following stimulation is still unknown. To address this temporal characteristic, Clennell et al. (2021) investigated the excitability profile of ultrasound-stimulated neurons following the sonication sessions. The authors first subjected cultured rat cortical neurons to a 40-second 200 kHz pulsed US stimulation then made an electrophysical analysis in a recording chamber.

The authors reported an increase of 32 percent in mean spike frequency in US-stimulated neurons compared to control cell levels within two hours post stimulation. For a longer interval following stimulation (6 to 8 hours), the mean spike frequency in US-stimulated cells was 44 percent greater compared to sham-stimulated neurons. For a time interval of 12-14 hours between sonication and excitability testing, the mean spike

frequency did not significantly change between US-stimulated cells and sham cells. A similar result occurred for a delay of 24-26 hours.

The results also showed no significant effect of ultrasound on resting membrane properties. The data indicate that a brief ultrasound stimulus modifies neuronal excitability up to eight hours. In addition, there was no difference in the action potential voltage threshold between control and US-stimulated neurons. Still, there were differences in half-width, depolarization rate, and repolarization rate for up to eight hours, and eliminated in 24 hours following sonication. The latter results indicate that US affects action potential kinetics. In addition, the authors found no difference in pre-synaptic bouton diameter or post-synaptic density thickness regardless of time delay.

Regarding the mechanism by which neurons are sensitive to US, voltage-gated sodium channels and potassium channels play a key-role in action potential. The results showed changes in the waveform of action potentials in US-stimulated neurons, specifically the depolarization and repolarization rates, largely governed by sodium and potassium channels.

Yoo et al. (2018) also explored the long-term effects of ultrasound, where they stimulated the somatosensory areas of anesthetized rats. The sonication session lasted for 10 minutes; the somatosensory evoked potentials (SEP) were measured twice before sonication (5 minutes and 2 minutes before) and five times after sonication (at 5, 10, 15, 25, and 35 minutes). The time plots of the SEPs showed that the effect of US on the SEPs lasted for 35 minutes. However, the anesthetic protocol did not allow examining the offline effect for more than 35 minutes; redosing the rats confounds the results.

In the upcoming chapters, we elaborate on the aims of the thesis. The first aim was to explore the changes in acoustic intensity profile as a function of parameters. The

second aim was to investigate the extended effect of LIFUS targeting the sciatic nerve of anesthetized rats.

CHAPTER III

INVESTIGATING CHANGE IN ACOUSTIC INTENSITY WITH RESPECT TO US PARAMETERS

The thesis investigates the prolonged effect of LIFUS and its potential in treating chronic pain. US waves propagate either in pulsed mode or continuous mode. The medium in which they propagate and US parameters, defined in figure 4, alter the amount of energy (or intensity) that the waves deliver. Thus, the thesis first explores the effect of the following parameters on the magnitude of acoustic intensity: duty cycle (DC), fundamental frequency (FF), input voltage, and attenuation of medium.

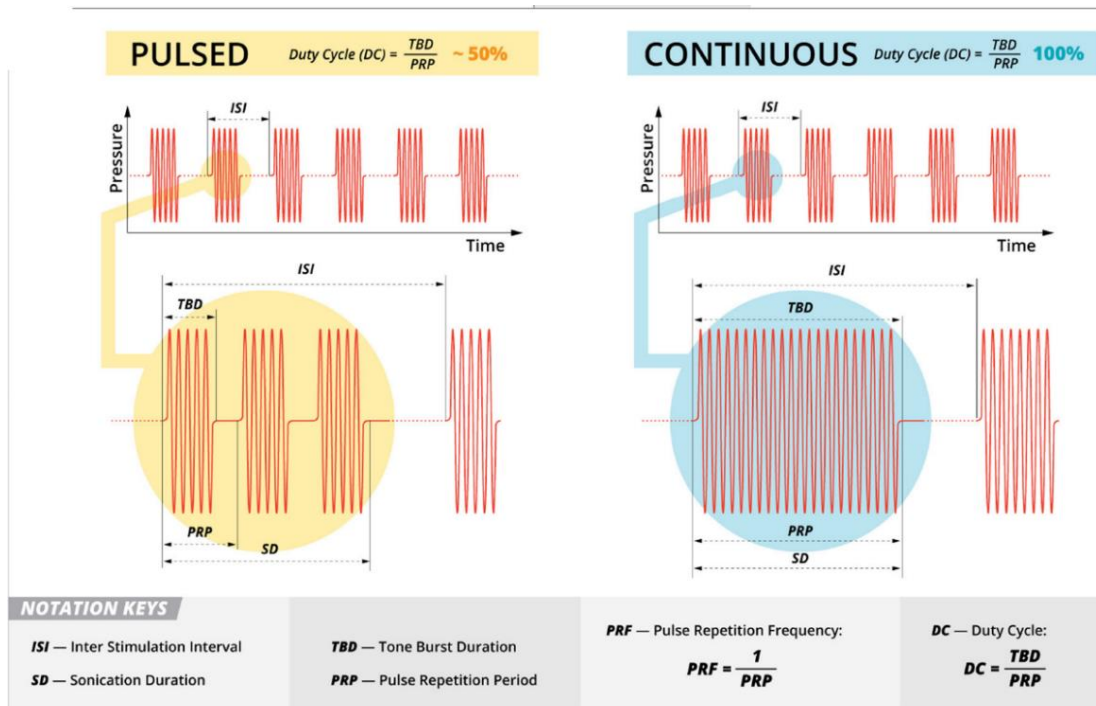


Figure 4: Definition of sonication parameters: inter-stimulus interval (ISI), sonication duration (SD), tone-burst duration (TBD), duty cycle (DC), and pulse-repetition period (PRP) (Dell'Italia et al., 2022). The signal propagates at a fundamental frequency (FF). Note: $TBD = CPP / FF$, and $BP = PRP$, where $CPP =$ number of cycles per pulse, and $BP =$ burst period. The BP represents the time interval separating each burst in pulsed signal. The DC represents the portion of the BP in which the amplitude of the signal is non zero. The PRF represents the number of pulses generated per second for a pulsed signal.

A. Experimental Setup and Procedure

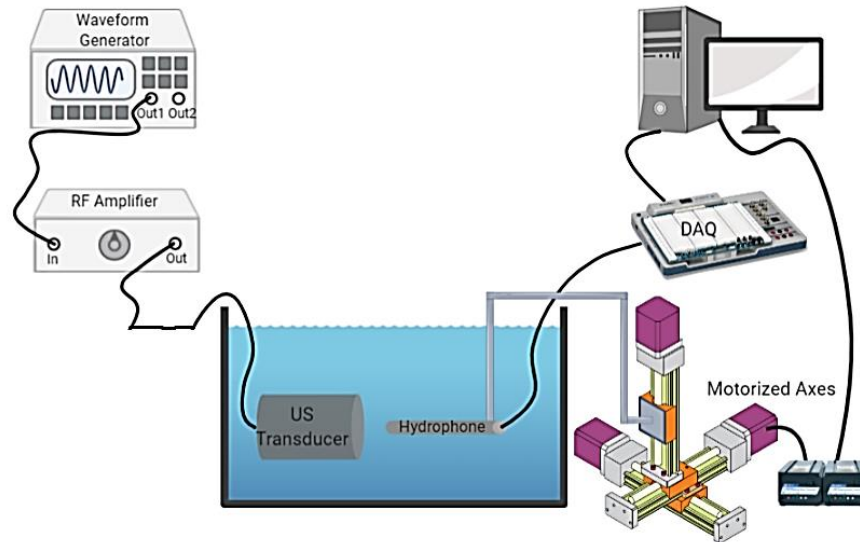


Figure 5: Schematic Diagram of Acoustic Profile Setup (edited from El Hassan, 2020)

To explore how the experimental parameters affect the intensity of the ultrasonic waves, we used a setup composed of the following (figure 5): a waveform generator that produces the electrical signal, an amplifier that increases the voltage of the signal, an immersible US transducer that converts the electrical energy to mechanical energy, a water bath in which the US waves propagate, a hydrophone that converts the mechanical energy of the US to electrical energy (or voltage measurements), a data acquisition (DAQ) system, a computer to process data and compute the acoustic intensity, and a motorized axes system that allows the hydrophone to move in three dimensions and scan specific geometric volumes via a user-specified code. The properties of the tools enumerated are provided in heading B of the Appendix.

During the experiments, the FF and BP were modified one at a time using the function generator. (Note that changing the BP or the number of cycles per pulse, CPP, changes the value of the DC). The hydrophone moved according to a code that controls the motion of the three motors and captured the voltage of the electrical signal at multiple locations relative to the transducer. (Motor 1 alters the motion of the hydrophone along the longitudinal axis of the transducer, motor 2 along the transversal horizontal axis, and motor 3 along the vertical axis or depth).

The intensity of the US waves was computed from the voltage recordings acquired and displayed in LabView. The intensity was then plotted as a colormap where the shades of the color represent the normalized spatial-peak pulse average intensity (ISPPA), i.e. the ratio of the local intensity to the maximum spatial intensity obtained in the scanned volume, with the maximum intensity (the spatial peak) being averaged across the TBD. (Heading A of the appendix describes the steps to calculate the acoustic intensity). The diameter of the focus was measured at full-width at half maximum (FWHM).

The colormap allowed visualizing the magnitude of the intensity and how the power propagates in the scanned volume for different sets of parameters. From these experiments, we determined the magnitude of the intensities in the pre-clinical studies in which US is implemented.

B. Results and Discussion

1. *effect of changing the DC by changing the BP*

The effect of changing the DC by changing the BP was explored. The DC represents the portion of the time interval in which the amplitude of the signal is non zero. (A 100 percent DC represents a continuous signal). The generator provided an amplitude of 225 mVpp. Table 1 provides the experimental parameters.

Table 1: sets of experimental parameters that explore effect of DC on intensity

FF (MHz)	CPP	TBD (microsecond)	BP (microsecond)	DC (%)
1.00	250	250	800	31.25
1.00	250	250	500	50
1.00	250	250	312.5	80

Figure 6 represents the colormap of the normalized spatial-peak pulse average intensities (I_{SPPA}) for FF= 1 MHz and DC= [31.25, 50, and 80 percent]. The shades of color correspond to a ratio that goes from zero to one.

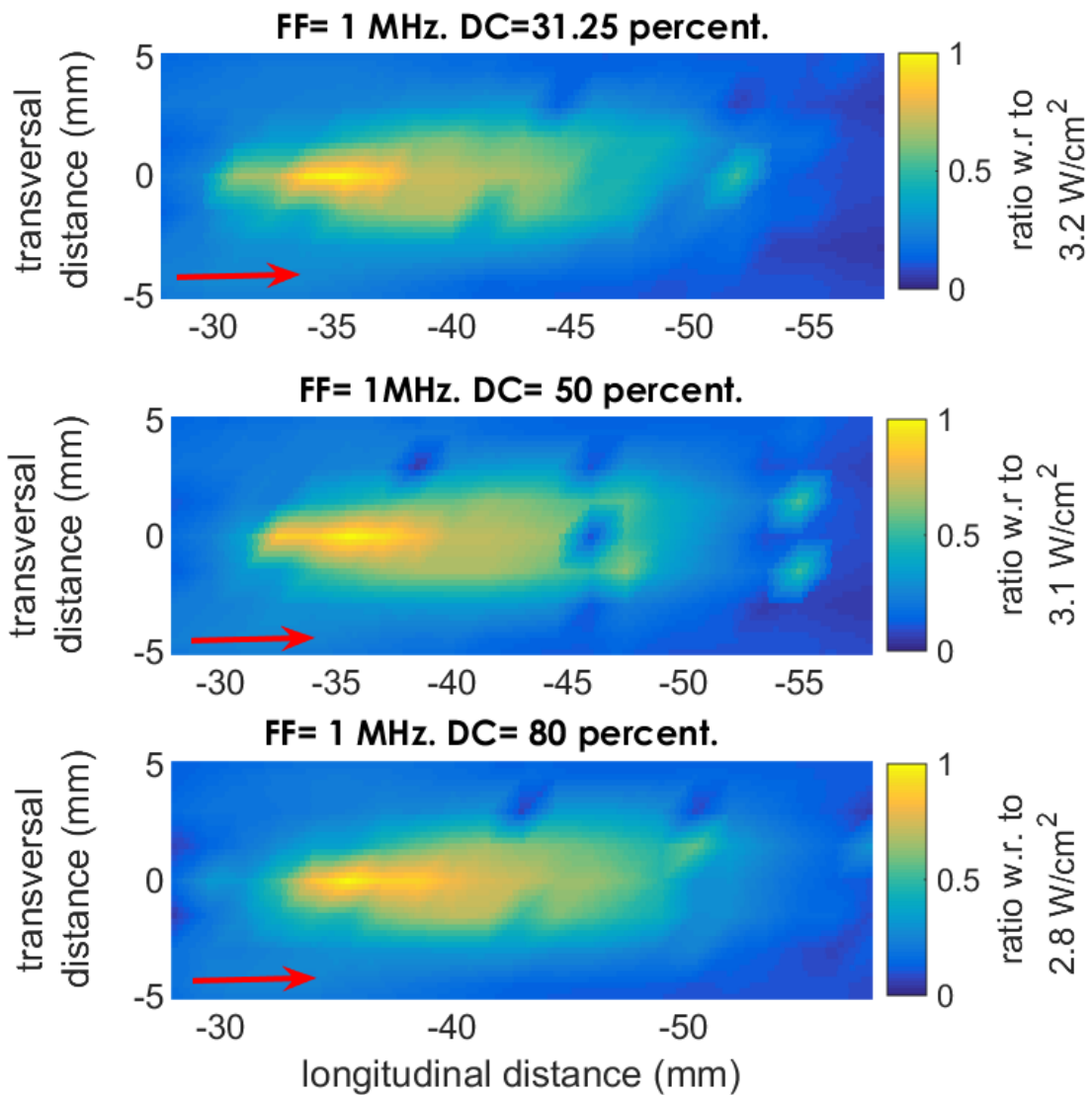


Figure 6: the profile of the normalized spatial-peak pulse average intensity (I_{SPPA}) for $FF= 1$ MHz at different DCs. (Max= approximately 3 W/cm^2). The red arrow indicates the direction of US waves. The Onda HNR-0500 hydrophone measured the voltage in the experiments of this subsection. A full-width version of each colormap of figure 6 is provided in Appendix C.

The intensity I_{SPPA} remained in the vicinity of 3 W/cm^2 for the chosen constant parameters and when increasing the DC by reducing the BP (figure 6). Thus, modifying the DC does not significantly alter the amplitude of I_{SPPA} . Only the spatial-peak temporal average intensity (I_{SPTA}) is altered, where the latter entity is expressed as: $I_{SPTA} = DC * I_{SPPA}$. The diameter of focus was 4 mm when measured at FWHM.

Table 3 provides the summary of results for each set of parameters.

Table 2: summary of the results of acoustic profile experiments.

FF (MHz)	DC (%)	Maximum I_{SPPA} (W/cm²)	Maximum I_{SPTA} (W/cm²)	Diameter of focus at FWHM (mm)
1.0	31.25	3.2	1.0	4
1.0	50	3.1	1.55	4
1.0	80	2.8	2.24	4

2. effect of raising the FF

Freije (2022) used the same setup in parallel with the experiments of this section. The author employed transducers having different center frequencies (1 MHz, 5 MHz and 7.5 MHz) but the same geometry and material (section B of the Appendix). The size of the focal point shrank and the power per unit area went up when increasing the FF.

3. effect of raising the input voltage that the function generator provides

The intensity was also computed for different input voltage amplitudes, modified using the function generator. In these experiments, the constant parameters were FF= 1MHz, CPP= 250, and BP= 500 μ s, with the amplitude of the signal at the function generator assigning the following values: 75, 150, and 225 mVpp. The same row was scanned. As expected, the intensity increased when raising the input voltage, since the former is function of the square of the latter. Figure 7 illustrates the results obtained when exploring the effect of changing the input voltage.

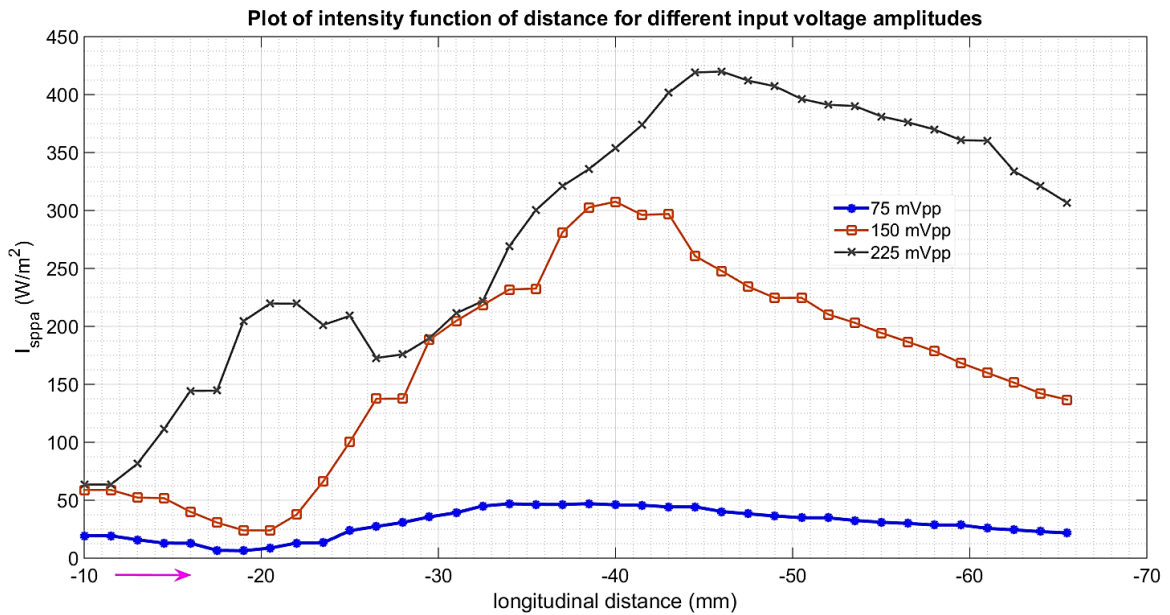


Figure 7: Plot of intensity function of longitudinal distance for input voltage amplitudes of 75 mVpp (blue curve with asterisk markers), 150 mVpp (red curve with square markers), and 225 mVpp (grey curve with 'x' markers). The arrow next to the bottom axis represents the direction of US waves. (FF= 1MHz, DC= 50 percent). The Sonic Concepts Y-104-023 captured the voltages in the experiments of this subsection.

4. effect of altering the medium properties

The tissues between the US source and target attenuate the intensity that US waves deliver. We thus explored the change in acoustic intensity when inserting a gelatin-based tissue-mimicking phantom between the transducer and hydrophone. These experiments aimed at determining the attenuation coefficient of the gelatin, and exploring how increasing the mass of gelatin powder alters the attenuation coefficient of the phantom. We experimented with the following concentrations: 12.5, 20, and 24 percent; the percentage corresponds to grams of powder dissolved per 100 mL water.

The gelatin solution was refrigerated for 24 hours. (Appendix D provides the recipe). After removing the gelatin from the refrigerator, we measured its mass, thickness, length and width. We measured the mass once again before inserting it in a

frame, submerging it in water and positioning it in front of the US-emitting transducer (figure 9).

The same horizontal plane was scanned, twice with the 12.5 percent gelatin phantom, twice with the one with 20 percent, and twice with the one with 24 percent, and once without phantom. The generator emitted a signal of FF= 1 MHz, CPP=100, BP=125 μ s (DC= 80 percent), and amplitude 150 mVpp. The maximum I_{SPPA} was computed from the voltage measurements in each experiment with the assumption that the refrigerated gelatin has a density and speed of sound similar to those of water. The attenuation coefficient α was calculated using the following equation (Azhari, 2010, p. 94):

$$\alpha = -10 * (\log_{10} \left(\frac{I_{Ph}}{I_w} \right)) * \frac{1}{x}$$

Where α is expressed in dB/cm, I_{Ph} is the maximum I_{SPPA} computed in the presence of phantom between US source and receiver, I_w the maximum I_{SPPA} computed without phantom, and x the thickness in cm. (The intensities shall have the same unit to ensure a unitless ratio).

In another date, a whole volume was scanned, once in water, and once with 12.5 percent gelatin phantom.

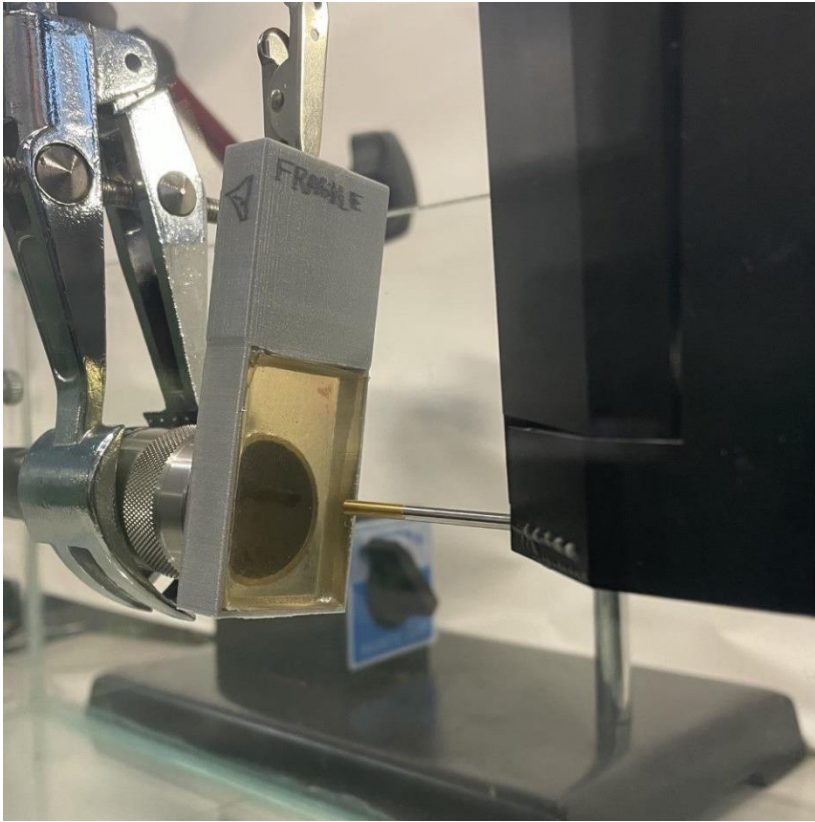


Figure 8: refrigerated gelatin inserted in a frame and positioned in front of the US source.

Adding more gelatin powder to the solution made the gelatin-based phantom more acoustically attenuating, i.e., the US waves transfer less power per unit area (figure 9). The attenuation coefficient rose because of the increase in concentration (figure 10). Figures 11 and 12 allow visualizing, respectively, the intensity drop per plane following the increase in concentration, and the drop per volume after inserting a phantom between the source and the receiver. The experiments corresponding to figures 10 and 11 were made in a different setting than the experiments corresponding to figures 12.

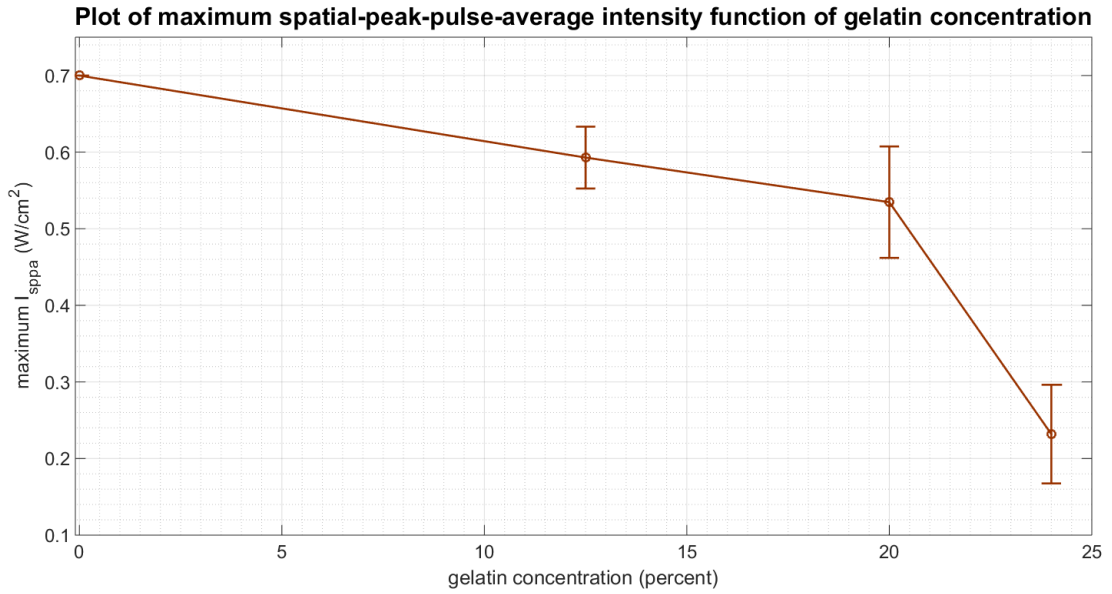


Figure 9: Plot of spatial-peak pulse-average intensity function of concentration. The error bar corresponds to one standard deviation. A zero concentration corresponds to propagation in water.

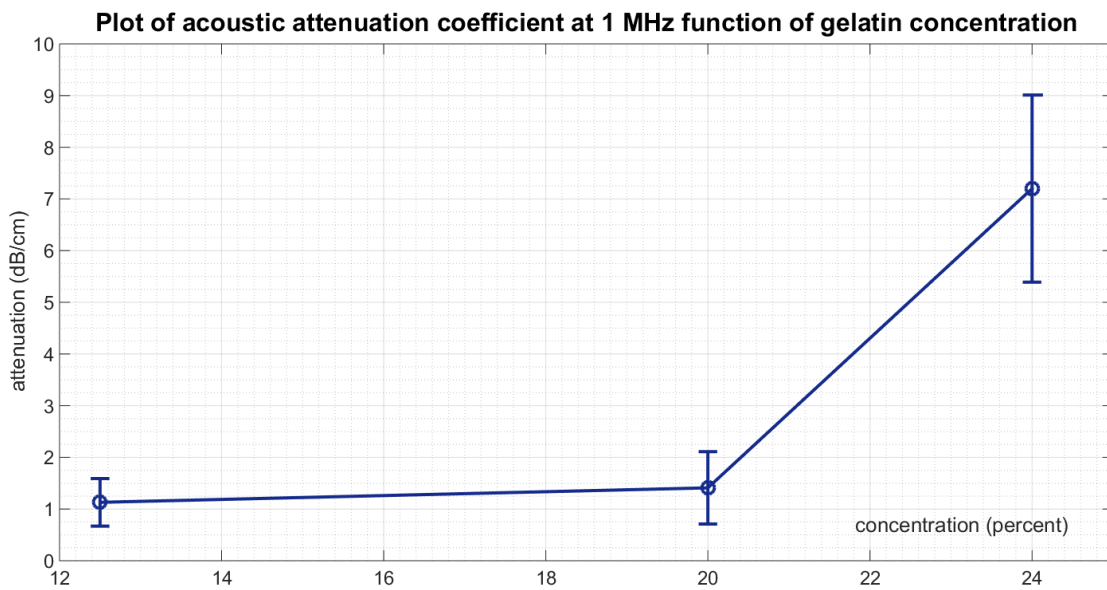


Figure 10: Plot of attenuation coefficient of gelatin-based tissue mimicking phantom function of gelatin concentration. The error bar represents one standard deviation.

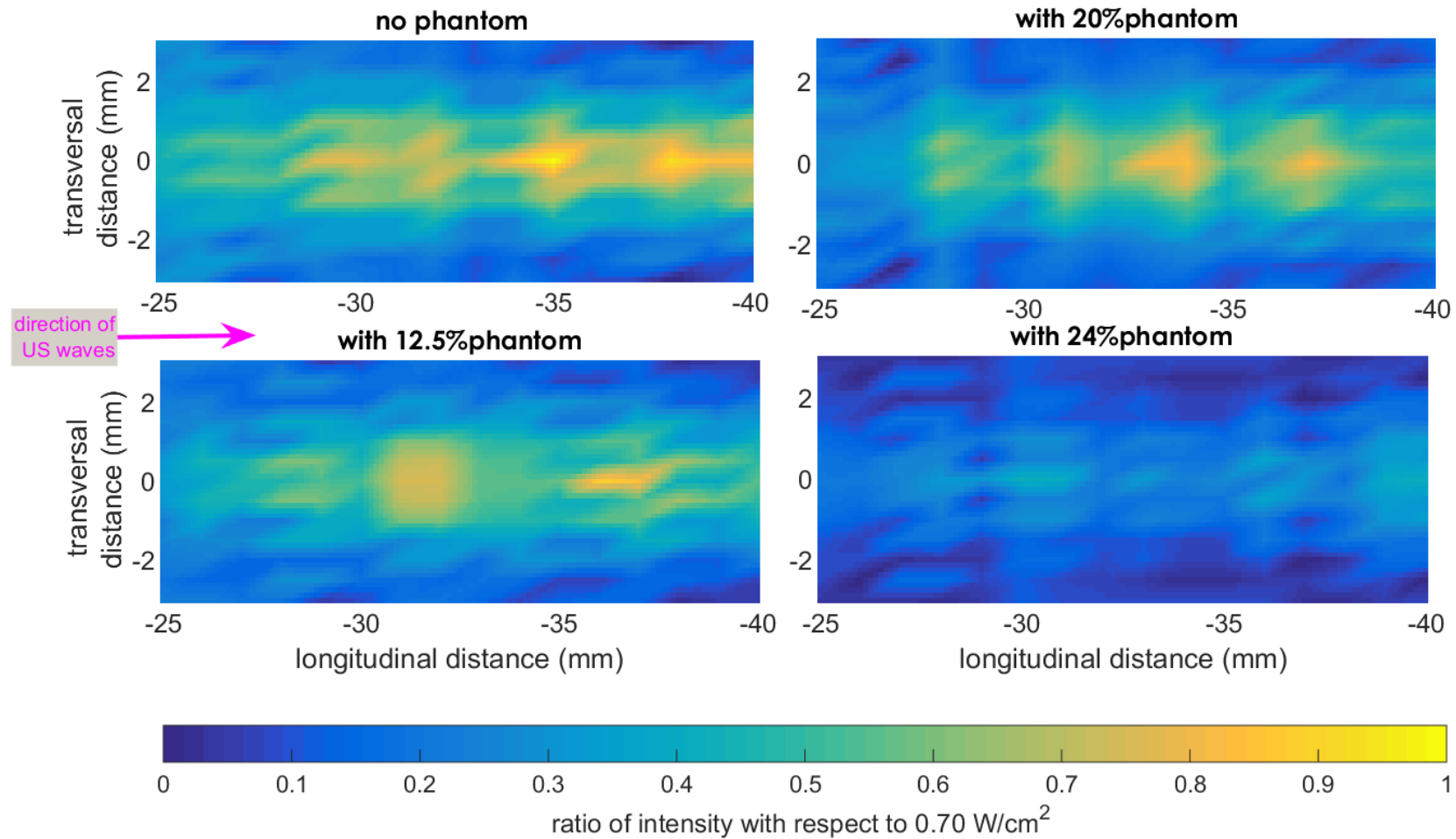


Figure 11: colormaps of normalized ISPPA for each gelatin concentration where the shades of color correspond to the ratio of the local intensity with respect to ISPPA in water (without phantom). Maximum local intensities are 0.70 W/cm² in water, 0.62 W/cm² with 12.5 percent gelatin phantom, 0.58 W/cm² with 20 percent gelatin, and 0.30 W/cm² with 24 percent gelatin.

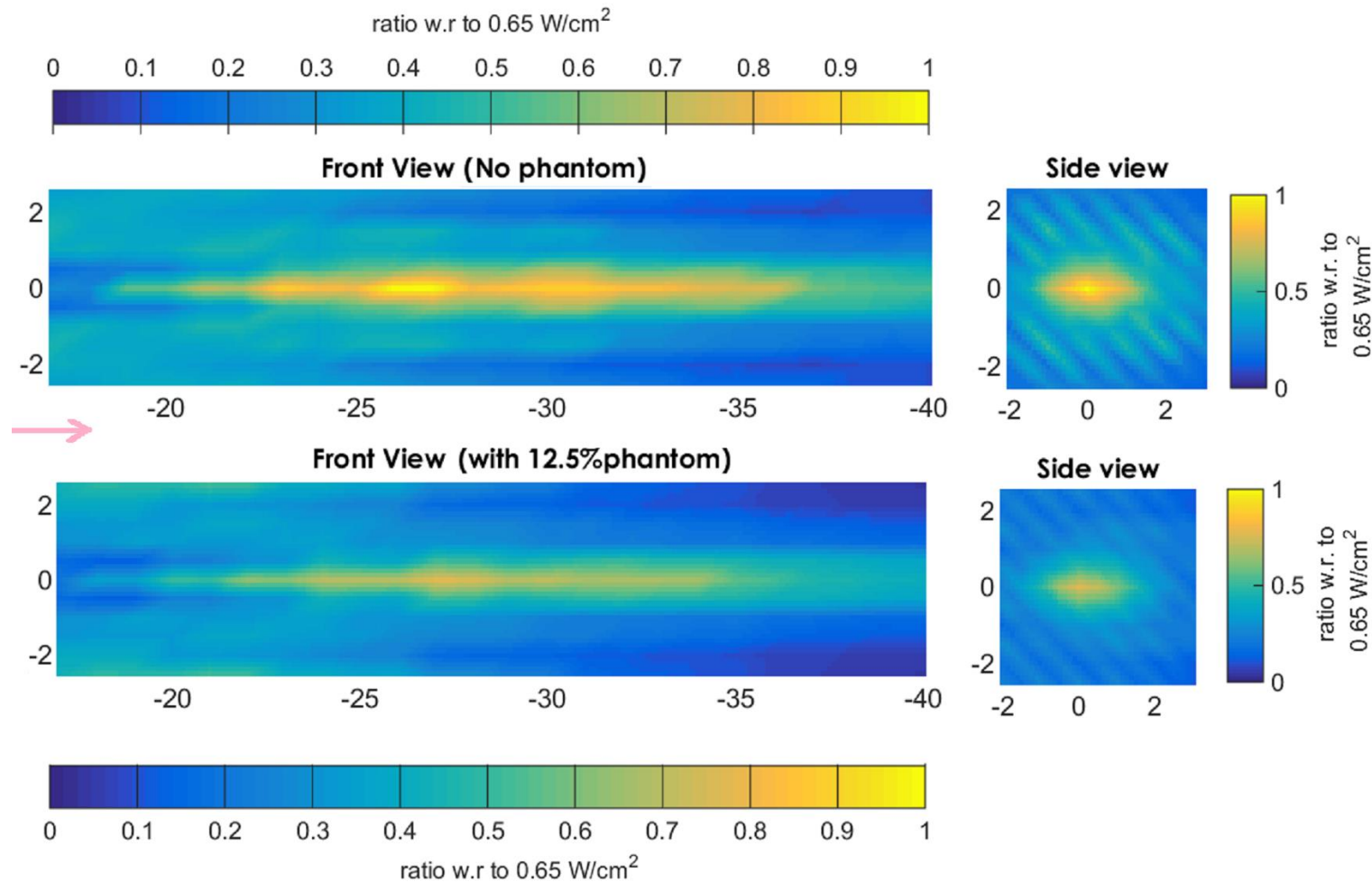


Figure 12: colormap of normalized ISPPA where the shades of color correspond to the ratio of the local intensity with respect to ISPPA in water (without phantom). Maximum intensities are 0.65 W/cm^2 in water, and 0.50 W/cm^2 with 12.5 percent gelatin phantom. The arrow indicates the direction of US waves. In the side view map, the direction of US is into the page.

The tissue-mimicking gelatin phantoms also underwent compression tests to determine their Young's modulus. For each gelatin concentration, ten cylindrical specimens (diameter= 8 mm and height= 8 mm) were compressed at a displacement rate of 0.1 mm/s up to a maximum strain of 0.4 mm/mm. The mean Young's modulus was calculated and plotted as function of concentration (figure 13). As expected, the gelatin with higher concentration is stiffer than the less concentrated. Figure 14 shows the stress-strain curve of three specimen at 12.5, 20 and 24 percent concentration.

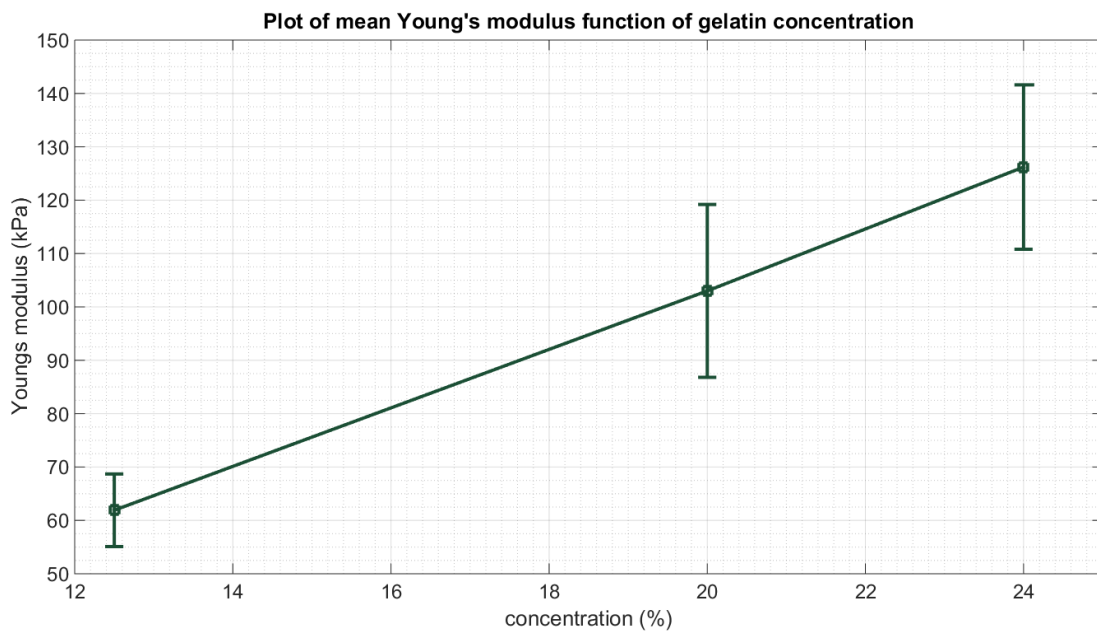


Figure 13: plot of Young's modulus of the gelatin-based tissue mimicking phantom function of gelatin concentration. The error bar represents one standard deviation.

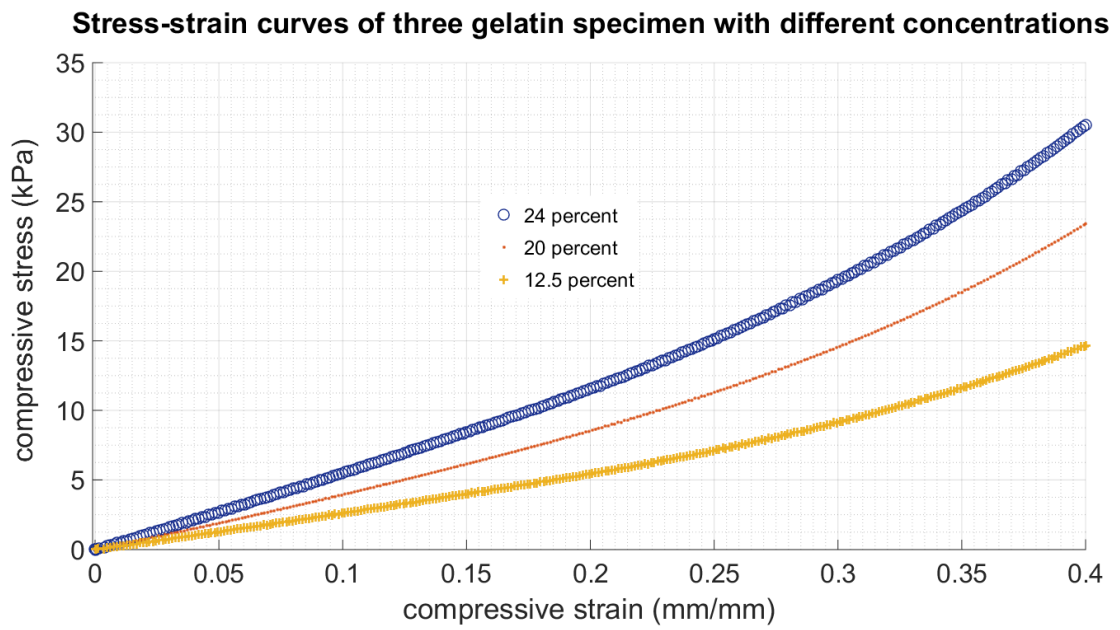


Figure 14: Stress-strain curve of three gelatin-based tissue mimicking phantom specimen with concentrations of 12.5, 20 and 24 percent. Displacement rate= 0.1 mm/s. Stopping condition: maximum strain of 0.4 mm/mm.

5. Similarities between tissues covering the sciatic nerve and gelatin phantom

The attenuation coefficient of tissue is either determined directly from previous studies and/or using the following equation (Azhari, 2010, p.98):

$\alpha = a \cdot (f^b)$ where f is the fundamental frequency in MHz.

To reach the sciatic nerve non-invasively, US waves must propagate through skin and then through skeletal muscle fibers. Skin is composed of three layers: the epidermis (outmost layer), dermis, and hypodermis. These layers have attenuation coefficients at 1 MHz of 0.44, 0.26, and 0.60 dB/cm respectively (Chen et al., 2016), which are of the same order of the attenuation coefficient of gelatin phantoms of concentrations less or equal to 12.5 percent. Muscle fibers attenuate acoustic waves by 1.09 dB/cm at 1 MHz (Cu;jat et al., 2010), which is of the same order of the attenuation of gelatin phantoms of concentrations between 12.5 and 20 percent (figure 10).

Regarding mechanical properties, skeletal muscles have Young's moduli ranging from 5 to 170 kPa, depending on the type of muscle (Guimarães et al., 2020). As for the skin covering the back of the thigh, Jacket et al. (2017) reported a value of 61 kPa. Hence, the stiffness of thigh skin and skeletal muscle are similar to those of gelatin of concentration between 12.5 and 20 percent (figure 13).

The outcomes of all the mentioned experiments allowed proceeding to the next chapter whose aim is to investigate the potential of LIFUS in prolonged or extended neuromodulation. The parameters explored in this chapter are employed in the upcoming chapter.

CHAPTER IV

INVESTIGATING THE PROLONGED (OR OFFLINE) EFFECT OF LIFUS TARGETING THE SCIATIC NERVE OF ANESTHETIZED RATS

The thesis aims at exploring the potential of LIFUS in the treatment of chronic pain by investigating the extended effect of LIFUS targeting the sciatic nerve of anesthetized rats receiving electrical stimulation that simulates chronic pain.

A. Materials and Methods

1. Animals

The experiments were performed on five (n=5) Sprague-Dawley male rats weighing between 273 and 319 grams on the days of the treatment.

2. Animal preparation

First, the rat would have its mass measured. A sufficient dose of ketamine and/or xylazine is injected based on the mass. Once anesthetized, the rat will have hair covering the limb shaved. After cutting through the shaved skin and the biceps femoris muscle, the sciatic nerve is exposed. The fat covering the sciatic nerve is removed. A silver electrical stimulating electrode is hooked to the nerve. The US-emitting transducer is positioned above the exposed nerve after being coupled with a cone filled with ultrasound gel (figure 15). A needle electrode is inserted in the gastrocnemius muscle to measure its electrical activity (the electromyogram or EMG) in response to the electrical stimulation. The ground electrode is attached either to the skin or to the testicle.

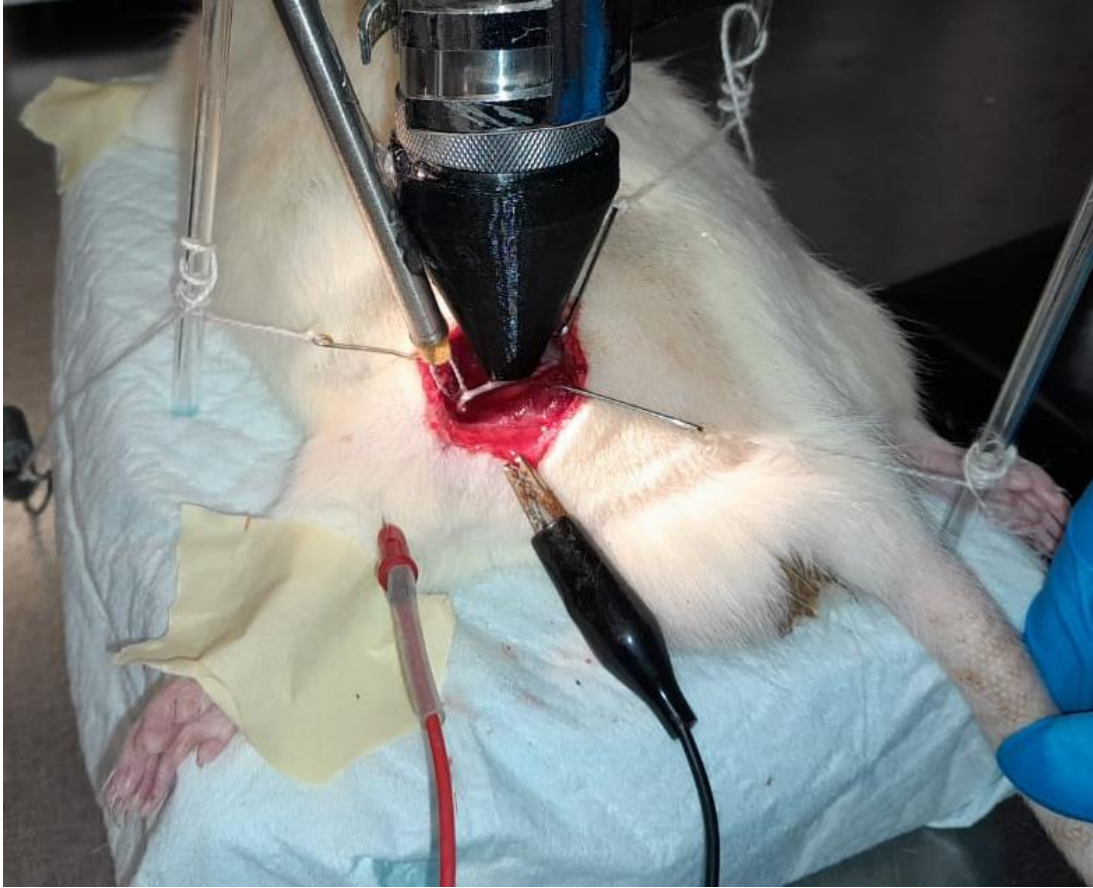


Figure 15: Photo of experimental setup. The stimulating electrode is hooked to the exposed sciatic nerve. The transducer is coupled with cone filled with ultrasound gel that serves as a medium for propagation.

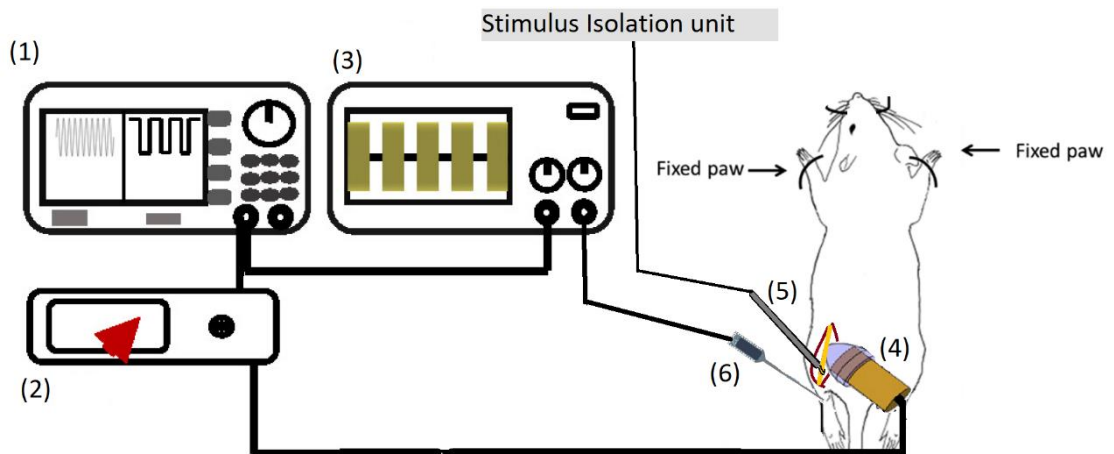


Figure 16: schematic of the animal experiment (components of figure extracted from Coutinho et al., 2020 and Liu et al., 2021). (1) function generator. (2) amplifier. (3) oscilloscope. (4) transducer targeting the exposed sciatic nerve. (5) stimulating electrode hooked to nerve. (6) EMG electrode inserted in gastrocnemius muscle.

3. *Ultrasound parameters*

The other end of the transducer is connected to the output of the amplifier whose input is connected to the function generator (figure 16). Their properties are provided in heading B of Appendix, as they are the same generator and amplifier used in the previous chapter. The function generator allows altering the FF of the signal, its amplitude, CPP, and BP, with the DC being function of both CPP and BP.

In the experiments of this chapter, we used an unfocused immersion transducer from Mana Instruments of outer diameter 25 mm (E0525-SU) to which a cone was coupled. The transducer has a center frequency of 0.5 MHz. The cone has a tip inner diameter of 2 mm and a distance from the face of transducer to tip of 30 mm. The cone allows the convergence of the US waves.

The SD and BP are modified one at a time to explore the offline effect of US on the sciatic nerve. The number of cycles (CPP) and amplitude of the signal remain the same. The choice of altering the DC and the SD is based on the results of Zou et al. (2020) and Fomenko et al. (2020).

When targeting the skull of epileptic monkeys, Zou et al. (2020) experimented with the following SDs: 5, 15, 30, and 60 minutes. The extracranial I_{SPPA} was of the order of 120 W/cm^2 and I_{SPTA} of the order 1.5 W/cm^2 . Their results showed that a session lasting for 15 minutes significantly reduced the duration and number of seizures up to 7 hours following the end of the session and more efficiently than other SDs.

As for Fomenko et al. (2020), they targeted the primary motor cortex of healthy human subjects. The extracranial I_{SPPA} was of the order of 9 W/cm^2 and the DC 10, 30 or 50 percent. The SDs were 0.1, 0.2, 0.3, 0.4 and 0.5 seconds. The results showed that

varying the DC and the SD (one at a time) significantly suppressed the amplitude of the motor evoked potentials (MEPs).

Table 4 summarizes the experimental parameters where ISPPA corresponds to the intensity at the tip of the cone.

Table 3: set of experimental parameters where US targets the sciatic nerve. A DC of 100 percent represents a continuous pulse. FF= 500 kHz. CPP= 125. TBD= 250 microsecond. Amplitude of signal at function generator output= 180 mVpp.

Mass of rat (g)	BP (μs)	SD (s)	DC (percent)	I_{SPPA} (W/cm²)	I_{SPTA} (W/cm²)	I_{SPTA}*SD (J/cm²)
283	312.5	30	80	1.4	1.12	33.60
	500	30	50	1.4	0.70	21.00
	800	30	31.25	1.4	0.44	13.13
276 or 312	312.5	60	80	1.4	1.12	67.20
	500	60	50	1.4	0.70	42.00
	800	60	31.25	1.4	0.44	26.25
286 or 319	312.5	90	80	1.4	1.12	100.80
	500	90	50	1.4	0.70	63.00
	800	90	31.25	1.4	0.44	39.38

4. Experimental procedure

Each experiment went as follows: First, we turn to 5 volts the knob that controls the amplitude of the electrical stimulation with the switch being turned off. We then start by recording the stimulus, the output of the function generator, and the muscle activity (sampling rate of 12.5 kHz or 12500 measurement per second). After 10 seconds, we turn to “on” the switch that controls electrical stimulation. The nerve is stimulated at a frequency of 2 Hz or 2 pulses per second where each pulse lasts for 2 milliseconds (duration= 2ms). After 30 seconds of electrical stimulation (at time= 40 seconds), we press the “signal on” button in the function generator. The nerve receives both electrical and ultrasound stimulation for a duration of 30, 60, or 90 seconds as

mentioned in table 4 and illustrated in figure 18. By the end of the SD, we press “signal off” such that the transducer stops emitting US waves. The nerve continues to receive an electrical stimulus for five minutes after cessation of sonication. Beyond this duration, we flip to “off” the switch of electrical stimulation. After 10 seconds of no stimulation, we stop recording the muscle activity.

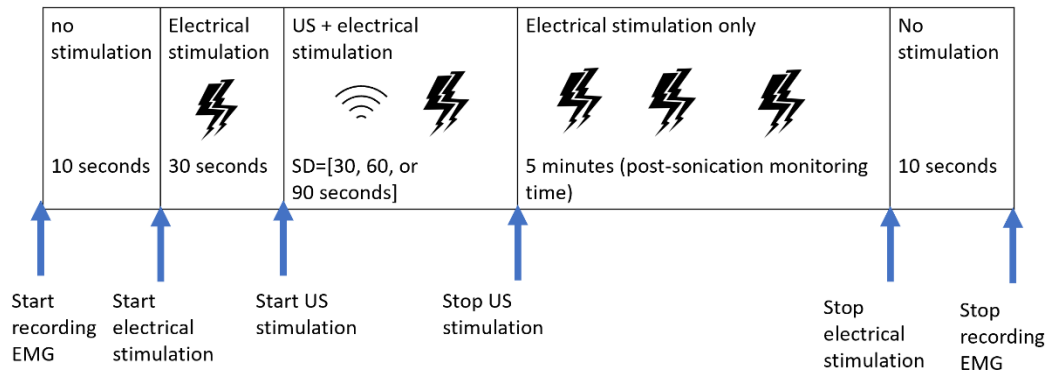


Figure 17: Experimental procedure. The electrical stimulation parameters are: amplitude= 5 volts, frequency= 2 Hz, duration of pulse= 2 ms, and delay = zero ms.

The impedance of the gastrocnemius muscle is not only function of morphological changes but also of biochemical and physiological features (Countinho et al., 2020). Biochemical features include the energy producing processes in which adenine triphosphate (ATP) molecules are supplied and hydrolyzed, and ions accumulated. When electrical stimulation starts, the muscle switches from rest to rapid motion requiring the consumption of anaerobically produced ATP molecules. For a stimulation session of 5 minutes at a frequency of 2 Hz, the muscle is considered undergoing moderate-intensity medium-length exercise. Therefore, anaerobic, and aerobic energy-release processes occur in the muscle, where each process of them has a distinct total number of ATP moles produced and hydrolyzed (Hargreaves & Spriet, 2006, p.3).

Taking into account these features, the experimental procedure requires having a minimum 15 minutes of break between each trial when experimenting on the same rat. This gives the muscle sufficient time to relax, recover its storage of ATP-producing molecules, and avoid neuromuscular fatigue. The effect of US treatment would also decay in this break time.

5. *EMG data analysis*

The experiments give as outcomes three vectors: stimulus, signal emitted from generator, and EMG (figure 18). The computations were made for each 30-second interval or 60 spikes (frequency= 2 pulses per second) using MATLAB. For each spike or pulse in the EMG vector, the amplitude (global maximum minus global minimum) and area under absolute value of EMG (AUC) were computed after disregarding the stimulus artifact. From the 60 spikes, the mean values were calculated.

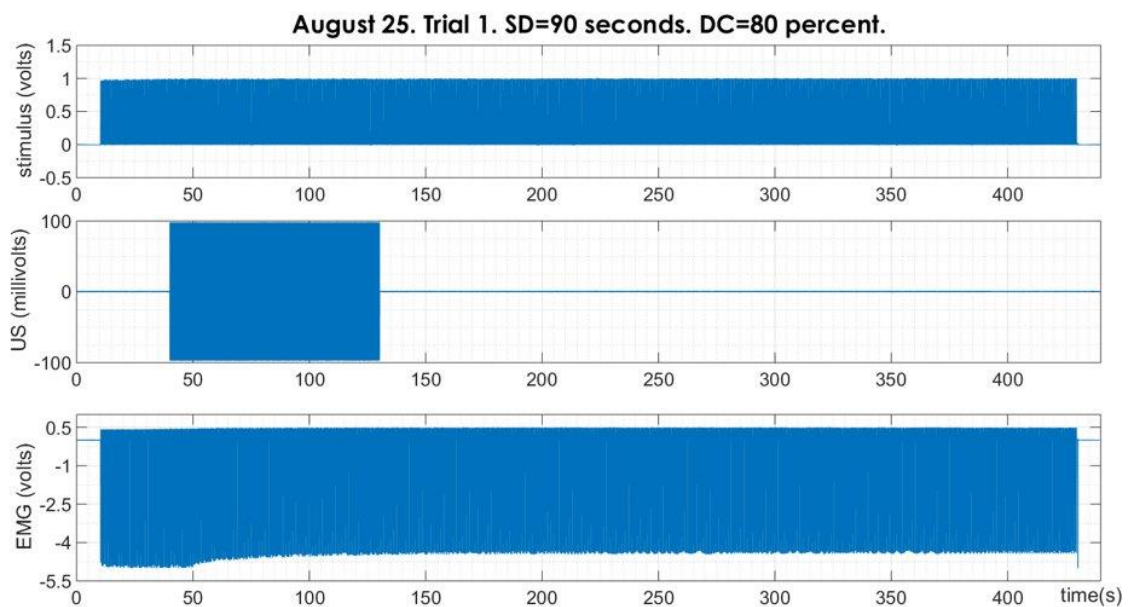


Figure 18: sample plots of stimulus, signal emitted by the generator before being converted to US, and amplified EMG.

The amplitude represents the maximum potential difference across the muscle (voltage peak-to-peak) or the maximum power per unit current (expressed in watts per amp). The AUC represents the voltage flux inside the muscle fibers or the energy per unit current circulating (expressed in volt*second or joules per amp).

B. Results

The mean amplitude and AUC in each 30-second interval were computed and plotted for each trial as a function of time, disregarding the two ten-second intervals in which there was no stimulus. Readers will find in Section E of the Appendix the time plots of average amplitude and AUC for each trial.

To determine the prolonged impact of treatment, we compare the amplitude and AUC in the last 30 seconds of each trial to those in the first 30 seconds of the trial (the interval preceding sonication). These regions are illustrated in figure 19 and denoted as region D and region A. A negative percentage change is translated as a drop in motion or an inhibitory effect of treatment, whereas a positive percentage change is translated as an increase in motion or excitatory effect of treatment.

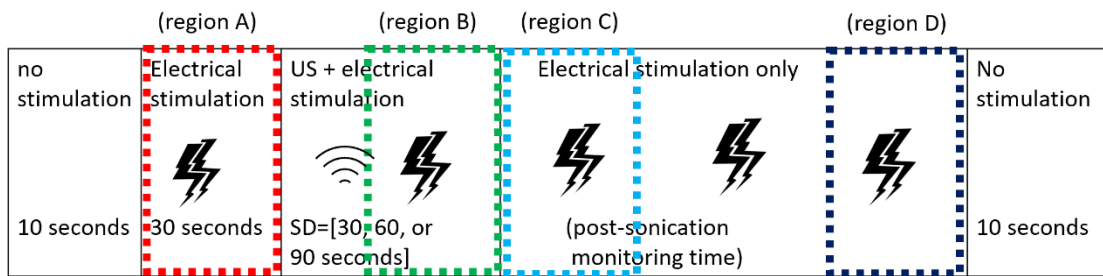


Figure 19: Region A corresponds to initial 30-second interval before onset of treatment. Region B is the last 30 seconds of the sonication duration where the nerve received both electrical stimulation and US treatment. Region D is the last 30-second interval in the trial before stopping EMG recording.

For trials having the same SD and DC, the average percentage change was calculated and plotted as function of DC (figure 20). For DCs of 31,25 and 50 percent, the percentage change in amplitude and AUC was between -3 and 3 percent for all durations. On the other hand, US treatment at a DC of 80 percent achieved greater modification in muscle activity compared to lower DCs, where the absolute value of the percent change was strictly greater than 4.7 percent.

Longer durations (60 or 90 seconds) were also more effective in reducing the muscle activity 5 minutes after the end of the treatment session. In contrast, treating for 30 seconds had a null effect (zero percent change) or an excitatory effect (positive percent change).

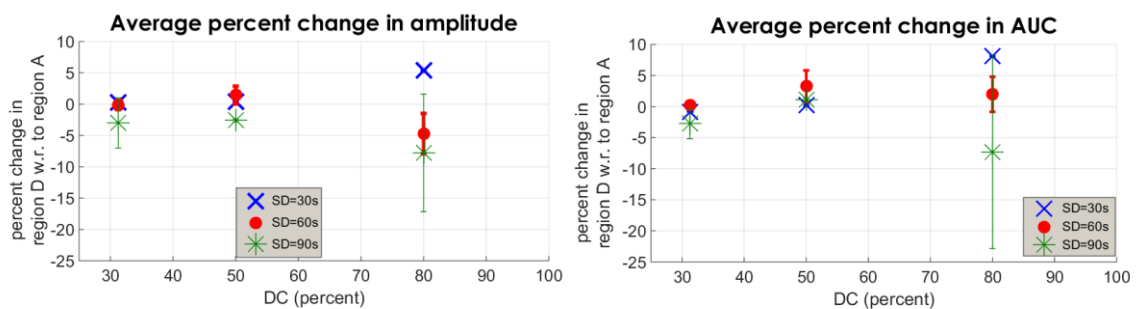


Figure 20: average percentage change in amplitude and AUC as function of DC, where percentage change is $=100 \cdot (\text{value in region D in current trial} - \text{value in region A in current trial}) / \text{value in region A in current trial}$. The error bar represents one standard deviation.

Each trial had its own combination of SD and DC, thus a distinct product of I_{SPTA} with SD, which is an energy-per-unit-area term (table 4). The plot of percentage changes as a function of energy (figure 21) showed scattering and a distinct response for each combination of DC and SD. Still, longer SDs and higher DCs proved to be more effective.

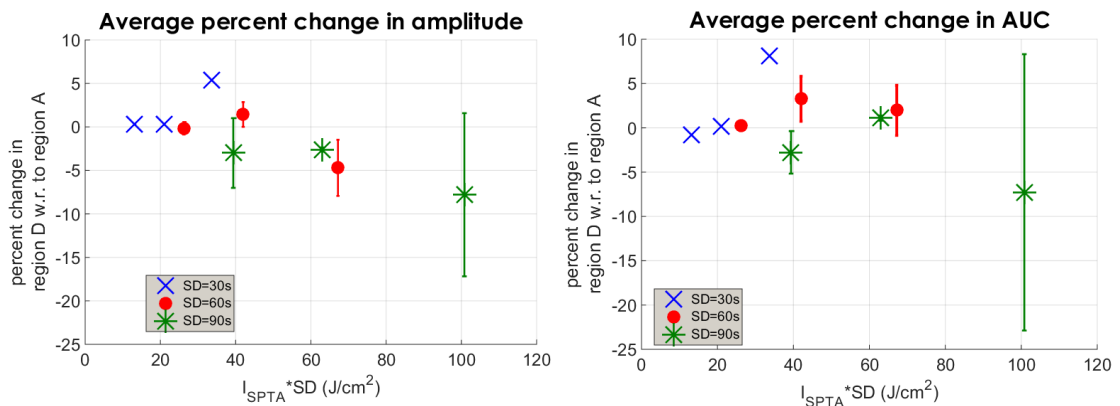


Figure 21: average percentage change in amplitude and AUC as function of $I_{SPTA} * SD$ for the same trial. The error bar represents one standard deviation.

The experimental procedure required taking a break of 15 minutes between each trial where the muscle rests. To determine whether the effect of US remains even after the 15-minute break, we compared the amplitude and AUC in region A of the trial that follows to those in region D of the current trial (figures 22 and 23).

Despite the variance illustrated in figures 22 and 23, the means assigned non zero values, implying that the effect of US phased out during the break between trials done on the same rat.

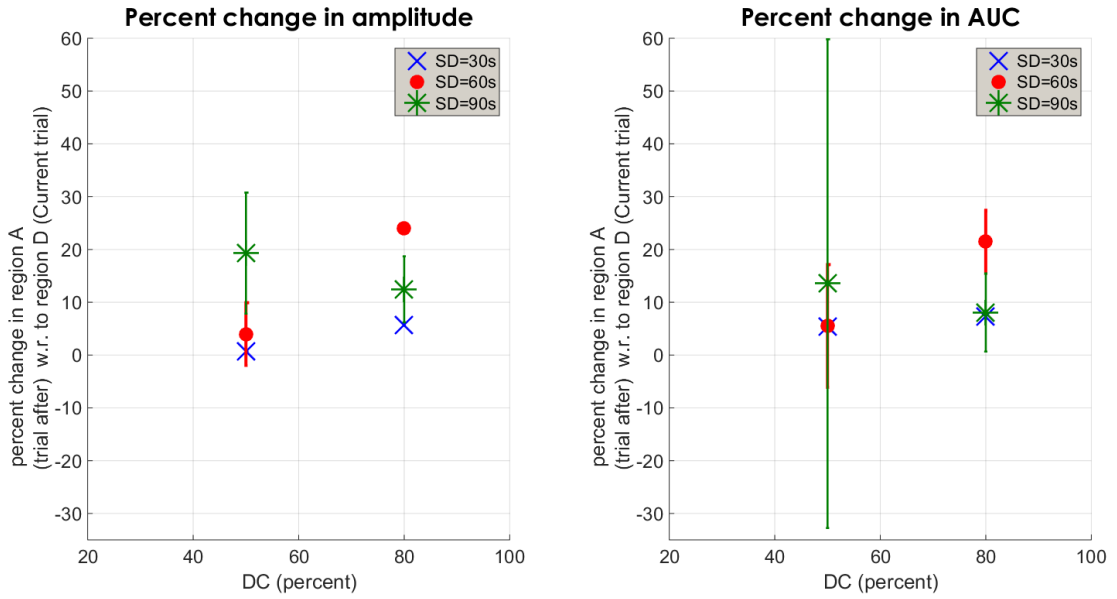


Figure 22: average percentage change in amplitude and AUC as function of DC, where percentage change is $=100 \cdot (\text{value in region A in trial after} - \text{value in region D in current trial}) / \text{value in region D in current trial}$. The error bar represents one standard deviation.

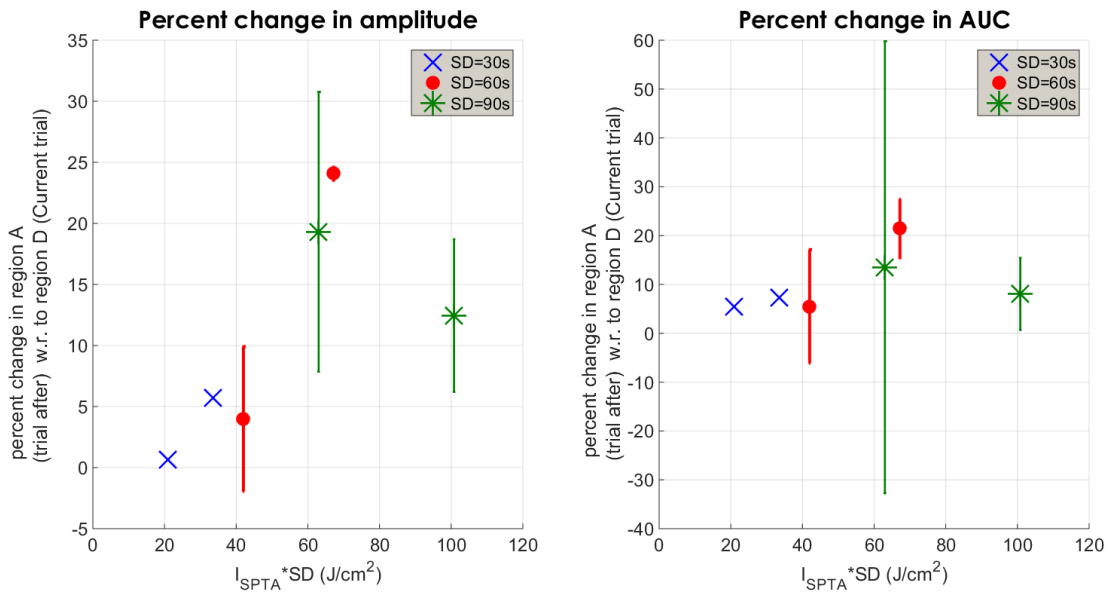


Figure 23: average percentage change in amplitude and AUC as function of $I_{SPTA} \cdot SD$ compared across trials on the same rat. The error bar represents one standard deviation.

To further determine how the treatment changed the muscle activity, the median of the frequency components of the EMG was computed and plotted using the Fast Fourier Transform function (figure 24). Consistent with the previous findings illustrated in figures 20 and 21, treating for longer SDs and higher DCs modified the frequency components of the EMG more, compared to lower durations. The trend was a shift towards a higher median frequency.

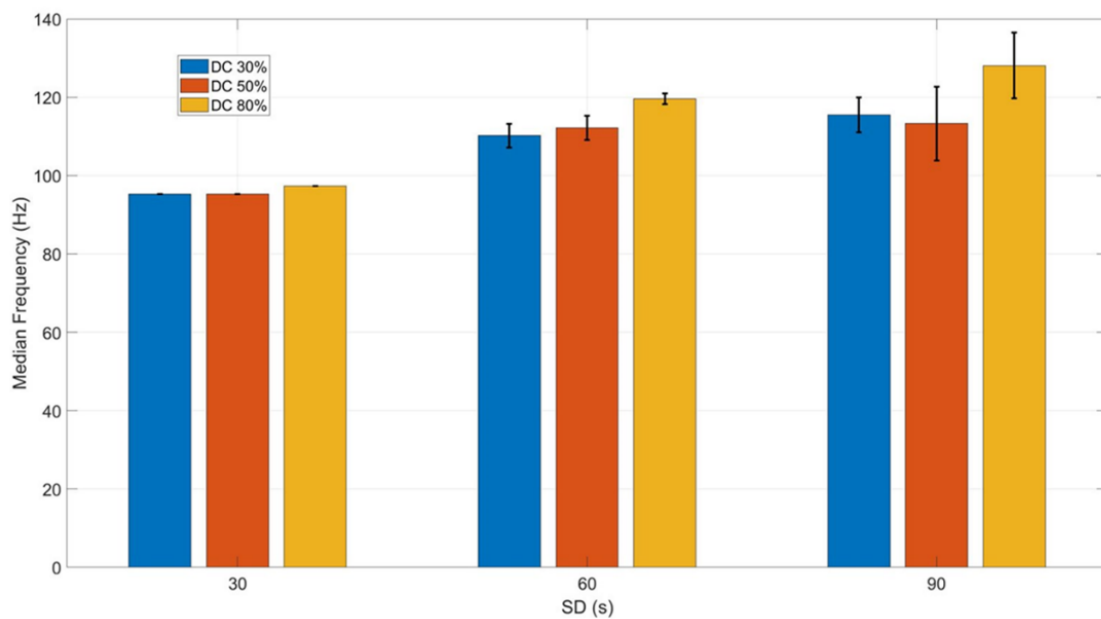


Figure 24: Median Frequency for each trial. One error bar represents one standard deviation. Credits: Heba Badawe.

Given that the twitching of the gastrocnemius muscle is analogous to the involuntary response to a thermal or mechanical stimulus, the change in the frequency components and amplitude implies that the treatment modulated the processes that occur in the reflex arc.

C. Discussion

1. *Potential of LIFUS in inducing prolonged change in neural activity*

The activity of the gastrocnemius muscle remained altered for up to 5 minutes post LIFUS treatment targeting the sciatic nerve, despite maintaining a constant electrical stimulus. The mean amplitude and AUC of the EMG spikes dropped following treatment (figures 20). The prolonged depression demonstrates the ability of LIFUS to modulate neural activity post treatment, i.e. after the end of the sonication session. The treatment also caused a shift in the median of the frequency components of the EMG measurements.

Typically, shifts in the median of the frequency of the EMG spectrum towards low frequency indicate fatigue (Naeije & Zorn, 1982). In our experiments, we saw a shift towards higher frequencies in experiments where US treatment was applied to the nerve. This is quite interesting given the reduced AUC of the EMG spikes. This possibly indicates that US is altering muscle fiber activation by activating new muscle fibers with different characteristics (higher conduction velocity) or altering the characteristics of the activated muscle fibers.

One of the aims of the study was to investigate the impact of varying US parameters, namely SD and DC, on prolonged activity. Our results showed that longer SDs and higher DCs induced a greater reduction in amplitude and AUC. Higher DCs correspond to a greater amount of power transfer per BP and a longer on-region in a single burst: the time interval during which the power is transferred is longer than the time interval in which the power is dissipated. Longer SDs imply a greater amount of total energy transfer per treatment session.

This finding is consistent with those of Fomenko et al. (2020) who targeted the primary motor cortex of healthy human subjects. The authors reported significant suppression of muscle evoked potential (MEPs) for longer SDs, and when increasing the DC by keeping a constant TBD and raising the PRF in a blocked manner with a 20-second break between sessions. (Raising the PRF is equivalent to reducing the BP)

In terms of energy transfer, a treatment of SD=90 seconds and DC=50 percent had an outcome similar to the treatment of SD =60 seconds and DC=80 percent (figure 21). This will raise the suggestion of using US at a higher power per unit area for a shorter duration. Nevertheless, extending the treatment session instead of transferring more intensity will avoid cell damage (Dedola et al., 2020).

Figures 20 and 21 showed variability in the mean percent changes at higher SDs, the latter can be attributed to variance from animal to animal.

The effect of sonication phased out during the 15-minute break between each trial on the same rodent (figure 22 and 23). Either the treatment remains effective for a period less than 15 minutes, or the state of the nerve before treatment dictates its response during and after sonication, i.e. a zero-stimulus pre-sonication could result in a no response during sonication. The latter assumption is based on the results of Nguyen et al. (2022) where pre-stimulation brain activity gated the response of the hippocampal region to tFUS.

US treatment targeting the sciatic nerve induced change in the movement of the gastrocnemius muscle. This modification is sustained even after US waves stop transferring power. (Appendix F describes the steps that lead to muscle movement following a stimulus). The mechanism that caused this prolonged effect is assumed to

be related to the mechanical properties of the tissue as a whole and the ion channels that regulate the events that occur during neuromuscular transmission.

2. Possible mechanisms through which sonication modulated muscle activity

a. identifying the type of US-induced neuromodulation: either synaptic or non-synaptic

The results reported in section B showed change in neural activity: targeting the sciatic nerve with US altered the motion of the gastrocnemius muscle during and post-sonication despite keeping the electrical stimulus constant. The change was either a rise in muscle activity or a drop.

A drop in EMG amplitude potentially means that fewer acetylcholine (ACh) receptors were activated after sonication. Given the location of the US target in the neuromuscular transmission process, it is possible that the prolonged change in the transmission occurred from the neuron side, i.e. in the axons of the neurons that make the sciatic nerve and/or at the presynaptic end.

Fewer/more ACh receptors were activated possibly because fewer/more ACh molecules were released in the extracellular space. This is in line with previous work showing that LIFUS alters the release of neurotransmitters (Liang et al.,2020). The work in question, previously summarized, proved that rabbits with STI receiving LIFUS treatment had lower concentration of inflammation markers at the injured site and higher levels of beta-endorphin compared to the untreated rabbits. Hellman et al. (2021) also noted a reduction of cytokines expression in rats with neuropathic pain up to 72 hours after LIFUS treatment.

The influx of calcium ions to the presynaptic terminal triggers the release of ACh, which leads to the assumption that sonication cut down the diffusion of calcium ions into the presynaptic end. Niu et al. (2022) attributed the long-term depression in rat

hippocampal activity on the ability of tFUS to change intracellular calcium concentrations, which is a direct modulator of synaptic plasticity. The authors correlated their findings with those of Yoo et al. (2022) who reported that US targeting cortical neurons enhanced calcium entry across the plasma membrane. However, in the experiments of this chapter, it is less probable that US waves directly manipulated the calcium channels: the intensity will be significantly attenuated when the waves travel from the sciatic nerve to the presynaptic end.

This finally raises the assumption that sonication caused non-synaptic modifications and altered the propagation of action potential along the axon, which is the first step of the processes that lead to muscle motion following stimulation of motor neuron. Future work, to be suggested in the upcoming paragraphs, will validate this hypothesis.

b. identifying the axonal components that responded to US treatment

The results of Clennel et al. (2021) (explained in section D of Chapter II) showed changes in the waveform of action potentials in US-stimulated neurons (up to 12 hours post-sonication). The changes were specifically in the depolarization and repolarization rates, largely governed by sodium and potassium channels. Kubanek et al. (2016) stated that US modulates the kinetics of the mechanosensitive sodium and potassium channels online and offline.

In the peripheral nervous system, voltage-gated sodium channels (also denoted Nav) are responsible for the initiation/propagation of action potential, autonomic regulation, and pain sensation. Mutations in these channels were linked with pain syndromes because of the change in the gating mechanics (Chahine, 2018, p. 53-54, 358).

Grubb et al. (2011) explained that the inactivation of axonal voltage-gated potassium channels (VGKCs) of the Kv1 family facilitates downstream neurotransmitter release. Regarding potassium channels and neuromuscular transmission, Vatanpour and Harvey (1995) reported that the blockade of potassium channels (whether voltage-gated or calcium-gated type) triggers ACh release, whereas Ambrosino et al. (2019) demonstrated that the activation of VGKCs of the Kv7 family inhibits the increase in concentrations of intracellular calcium ions. Wang et al. (2020) also provided evidence that VGKCs regulate transmitter release at the neuromuscular junction.

Kv7 and Kv1 channels are located at the nodes of Ranvier in myelinated motorneurons and at the axon initial segment. The former family serves as activity-dependent regulators of motor neuron excitability; activating the Kv7 channel during repetitive firing decreases the firing rate of motor neuron in response to prolonged depolarization input (Deardorff et al., 2021). Kv1 subunits have rapid kinetics in contrast to the slow time dependence of the activation of Kv7 subunit.

Gamper and Wang (2021, p. 236) stated that developing openers of the VGKCs of the Kv7 subunit serves as basis for therapy of epileptic seizures and chronic pain since loss of the function of this channel leads to neuronal hyperexcitability. Nav channels are also targets for the therapeutic treatment of chronic pain and epilepsy because of their essential role in rapid conduction of electrical impulses when activated (Chahine, 2018, p. 210). Zou et al. (2020) and Lin et al. (2020) reported that US treatment inhibited epileptic seizures in non-human primates.

Singh et al. (2022) mentioned that the mechanosensation of the Kv7 subunits contributes to neural plasticity. Morris & Juranka (2007) proved that Nav channels are

sensitive to mechanical stretching and that stretching modifies the activation and inactivation kinetics.

According to Dell’Itralia et al. (2022), mechanosensation is the conversion of mechanical energy into neural signals via sensory cells that have mechanosensitive ion channels that detect pressure. US waves cause reversible change in ion transfer by stretching these channels or activating them by particle displacement.

S. Zhang et al. (2022) modeled the propagation of the US wave in a linear, elastic, and isotropic material using Navier-Stokes equation expressed in terms of the particle displacement. Their simulations and experiments on tissue-mimicking phantom showed that the particle displacement is function of the acoustic radiation force (ARF) of US waves (in linear scale) and of the elastic properties of the tissue (in logarithmic scale). The ARF was expressed in terms of attenuation and instantaneous intensity.

In contrast, Azhari (2010, p. 95) explained that US waves should rather be considered propagating in a viscoelastic material, not perfectly elastic. In an elastic material, the input energy that causes reversible displacement is equal to the energy released when the pressure is unloaded; the stress-strain plot is a straight line (figure 25a). In a viscoelastic material, hysteresis occurs, where there is a discrepancy between the energy applied and the energy released when loading and unloading (figure 25b). The viscoelastic matter absorbs this energy difference.

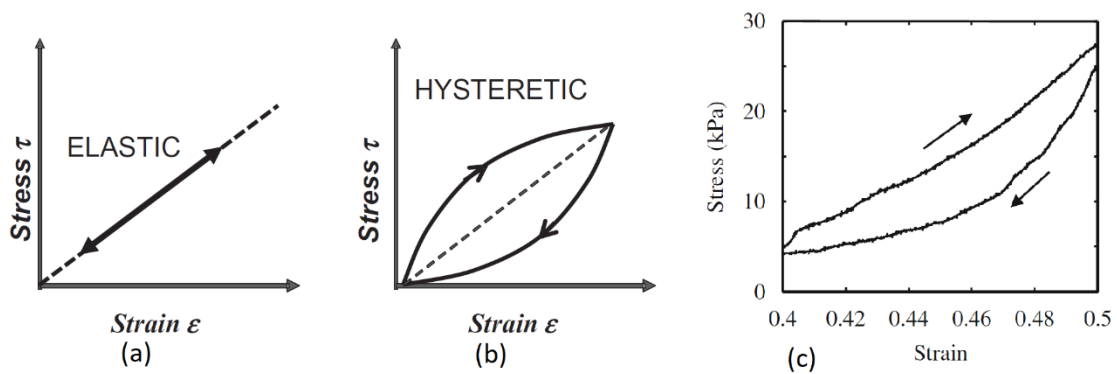


Figure 25: Stress-strain relationship for (a) an ideal elastic, (b) for viscoelastic matter (b) (Azhari, 2010, p. 96), and (c) for the sciatic nerve samples of Chen et al. (2010b) under cyclic loading.

c. modeling the strain that the US treatment caused

The rat sciatic nerve samples of Chen et al. (2010b) showed hysteretic behavior under cyclic loading (figure 25c), similar to the samples of Wong (2005) where the nerve's tensile elastic modulus changed with the change of strain rate. Therefore, the viscoelastic particles that make up the sciatic nerve can be represented as a spring-damper-mass assembly (Azhari, 2010, p. 96).

When a stress is applied to this assembly, the spring responds instantaneously and stretches, whereas the damper absorbs energy and applies a force that resists deformation and that is proportional to the strain rate (figure 26).

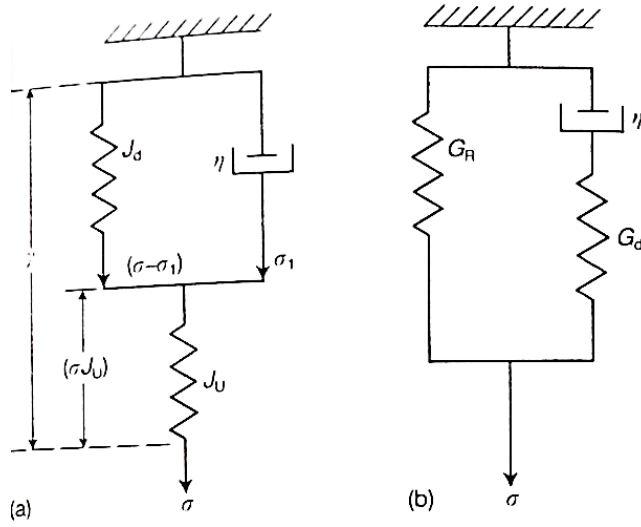


Figure 26: Zener model representing the viscoelastic material as (a) a spring in series with a Kelvin model, and (b) a spring in parallel with a Maxwell model (McCrum et al., 2001, p. 141). J_R and J_U are the time-independent compliances. $[\eta]$ is the damper coefficient. ($J_d = J_R - J_U$ is the time-dependent compliance). G is the stress relaxation modulus.

The equation that relates stress $[\sigma]$ to strain $[\gamma]$ and their derivatives in the Zener model illustrated in figure 26 is (McCrum et al., 2001, p.142):

$$\frac{1}{J_R} \left[\gamma + \tau_\sigma \frac{d\gamma}{dt} \right] = \sigma + \tau_\gamma \frac{d\sigma}{dt}$$

Where J_R and J_U are the time-independent compliances, J_d is the time-dependent compliance, $[\tau_\sigma]$ is the stress relaxation time constant ($\tau_\sigma = J_d * \eta$), and $[\tau_\gamma]$ is another time constant expressed as $[\tau_\gamma] = [\tau_\sigma] * J_U / J_R$. The damper coefficient $[\eta]$ is analogous to the viscosity of a fluid. The compliance $[J]$ is the inverse of the modulus $[G]$.

When the US waves generate an oscillatory shear stress in a linear viscoelastic material, the strain response at steady-state is also sinusoidal, but is out of phase with the stress (figure 27).

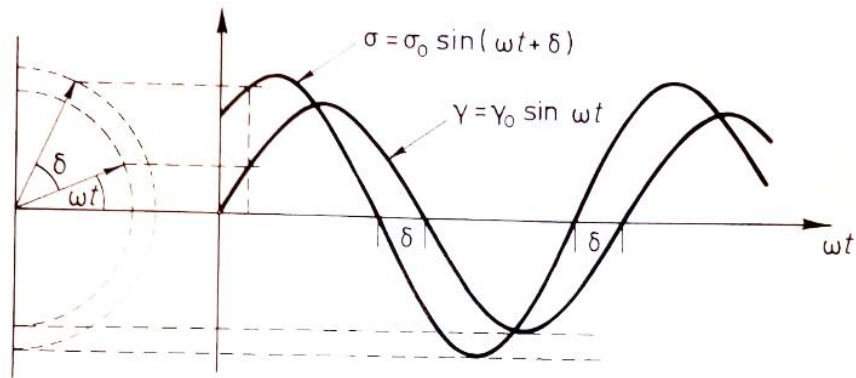


Figure 27: vector representation of an alternating stress leading a strain by a phase angle δ (McCrum et al., 2001, p. 129) at steady state. $[\omega]$ is the angular frequency. $[\sigma]$ is oscillatory stress. $[\gamma]$ is the oscillatory strain.

In the experiments of this chapter, the US waves propagated in a pulsed mode at a maximum I_{SPPA} of the order of 1 W/cm^2 and ion channels absorbed a portion of this power. VGKCs are tetramers (Gmayer & Wang, 2021, p. 5), which makes them a viscoelastic matter. Navs channels are also viscoelastic since they are composed of large chains of amino acids. (The figures in Appendix G illustrate respectively the structures of voltage-gated potassium and sodium channel).

During US treatment and in the on-region of the BP (during the TBD), US waves induced a sinusoidal stress in the nerve as a whole, including the channels, and caused strain.

$$\text{Stress } \sigma = \sigma_0 \sin(\omega t).$$

$$\text{Compliance } J(t) = J_R + (J_U - J_R) \exp(-t/\tau_\sigma).$$

The strain is modeled as linear viscoelastic under sinusoidal oscillations. Using the differential equation previously written and a procedure similar to McCrum et al. (2001, p. 167-168), the strain as a function of time is expressed as:

$$\begin{aligned} \gamma(t) = & \sigma_0 \left[J_R + (J_U - J_R) * \frac{\omega^2 \tau_\sigma^2}{(1 + \omega^2 \tau_\sigma^2)} \right] * \sin(\omega t) \\ & + \sigma_0 (J_U - J_R) * \frac{\omega \tau_\sigma}{(1 + \omega^2 \tau_\sigma^2)} * \cos(\omega t) \\ & - \sigma_0 (J_U - J_R) * \frac{\omega \tau_\sigma}{(1 + \omega^2 \tau_\sigma^2)} * \exp\left(-\frac{t}{\tau_\sigma}\right) \end{aligned}$$

Where $[\sigma_0]$ is the maximal stress, $[\omega]$ is the angular frequency, J_U and J_R are the time-independent compliances, J_d is the time-dependent compliance, and $[\tau_\sigma]$ is the stress relaxation time constant.

The first term of the equation represents the steady-state response in phase with the stress, the second term represents the steady-state response 90 degrees out of phase with the stress, and the third term of the equation is a transient that decays from the start of the oscillation. Palacio-Torrallba et al. (2015) used a similar equation when modeling the strain and reaction force in prostate tissue receiving a uniaxial sinusoidal force (figure 28).

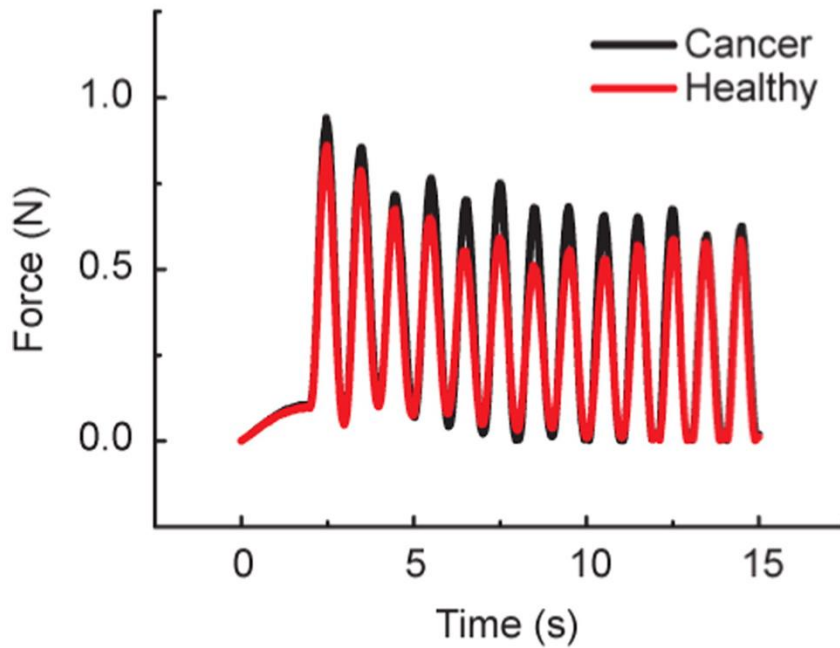


Figure 28: reaction force of prostate specimen receiving uniaxial sinusoidal force (Palacio-Torrallba et al., 2015). The reaction force starts with a transient response.

In the off-region of the BP and post-sonication, stress and its derivative are zero; strain in the channel decays exponentially according to the solution of equation 4.47 in McCrum et al. (2001, p.142):

$$\gamma(t) = \gamma_0 * \exp\left(-\frac{t}{\tau_\sigma}\right)$$

where γ_0 is the strain the instant of stress removal. For reference, the strain reaches 5 percent of its initial value within three time constants (at $t= 3*\tau_\sigma$) as illustrated in figure 29.

Several authors used the Zener model (figure 26) to determine the stress relaxation time [τ_σ] of animal tissue and the time-dependent stress relaxation modulus [G_d], also termed short-term modulus or transient modulus. Table 5 summarizes the values found in literature.

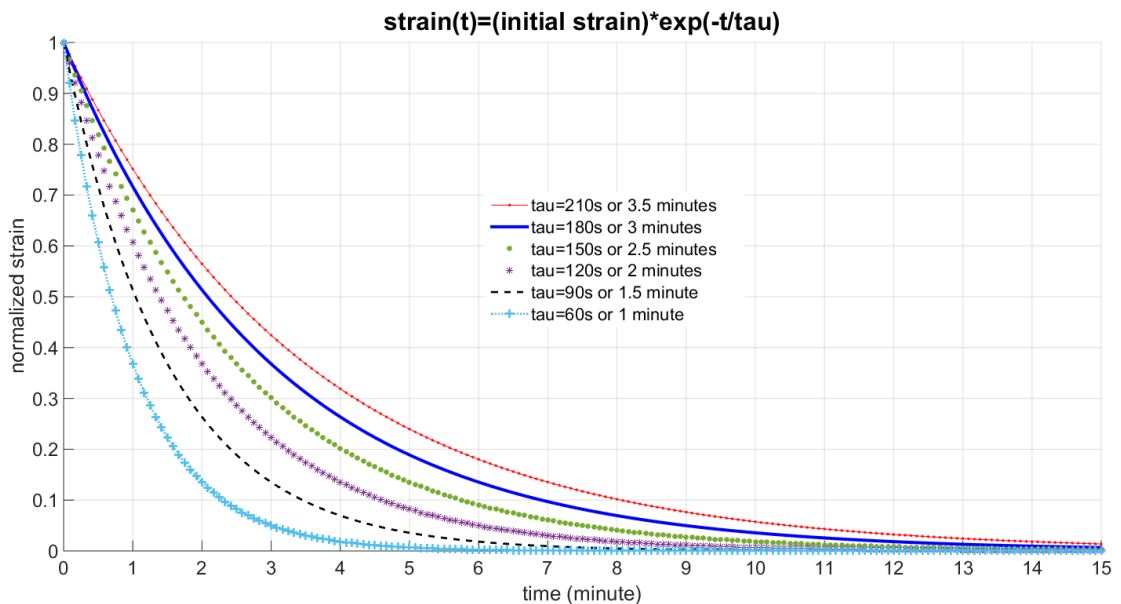


Figure 29: exponential decay of the strain of a viscoelastic material. The time constant varies from 60 seconds to 210 seconds.

Table 4: time-dependent moduli and relaxation time constants of animal tissues.

Tissue type	Time-dependent modulus (kPa)	Relaxation time constant (second)	Source
Rat liver	3	53	Maccabi et al. (2018)
Porcine liver	3	53	Maccabi et al. (2018)
Porcine optic nerve head	1.9 [1, 2.4]	214 [89, 921]	Safa et al. (2021)
Cancerous human prostate	2	10	Palacio-Torralba et al. (2015)
Healthy human prostate	4	5	Palacio-Torralba et al. (2015)
Healthy human pancreas	Not reported	93	Rubiano et al. (2018)
Cancerous human pancreas	Not reported	66	Rubiano et al. (2018)
Healthy rat sciatic nerve	Not applicable*	199	Chen et al. (2010b)

*Chen et al. (2010b) used a quasi-linear model.

d. coming up with the hypothesis explaining the change in muscle activity

From the references and models reported in the former subsection, we assume that US treatment modulated muscle activity as follows:

At the targeted area and in the on-region of the BP, the viscoelastic particles that make up the nerve absorbed the acoustic intensity and converted it to particle displacement and/or internal energy. This displacement stretches the mechanosensitive potassium and sodium channels through which ions diffuse during depolarization. The enhanced diffusion of sodium ions increases the firing rate, whereas the enhanced diffusion of potassium ions decreases it. This modification in the propagation of the action potential affects the rate at which ACh moles are rejected, since the arrival of the action potential to the presynaptic terminal triggers the release of ACh molecules into the extracellular space and causes muscle movement.

Post-sonication and in the off-region of the BP, the channels and the nerve as a whole remain stretched, where the strain decays exponentially because of the viscoelastic nature of the tissue and channels. Nav, Kv1 and Kv7 channels have their own molecular structures and viscoelastic properties. Hence, they will have distinct time constants ($\tau_{\sigma} = J_d^* \eta$).

As mentioned earlier, the inactivation (blockade) of Kv1 channels facilitates transmitter release, the activation of the Kv7 channel during repetitive firing decreases the firing rate of motor neuron in response to prolonged depolarization input, and the activation of Nav channels facilitates the propagation of action potential.

The rates at which the strains in channels return to pre-sonication state (the post-sonication strain rate) are function of the time constants and the strain at the instant of sonication cessation (the boundary condition). This explains why different combinations of DC and SD (time-dependent parameters) gave distinct experimental outcomes. Treating the sciatic nerve with US for 90 seconds or 60 seconds at a higher DC caused a drop in muscle activity, whereas a 30-second long treatment excited the muscle or had no effect.

Vasu and Kaphzan (2021; 2022) hypothesized that VGKCs and Nav channels are involved in the modulation of functioning of cortical neurons receiving transcranial direct current stimulation (tDCS). They validated the hypothesis by applying tDCS while locally blocking the Kv1 channels or sodium channels using selective drugs.

Demonstrating that Kv1, Kv7, and Nav channels are involved in US-induced modulation is achieved by using a similar procedure.

CHAPTER V

CONCLUSION AND FUTURE WORK

This work investigated the potential of LIFUS in modulating the sciatic nerve activity for an extended period of time. To achieve this, we explored the change in the power per unit area that the US waves transfer following the change in DC and the medium of propagation. Then, we investigated the offline effect of US treatment targeting, at different combinations of sonication parameters, the exposed sciatic nerve of anesthetized rats. The nerve was electrically stimulated to simulate pain sensation.

From the resulting EMG recordings and computations, we showed that the treatment successfully reduced muscle activity for up to 5 minutes after sonication cessation. We also found in this study that higher DCs and longer durations caused the greatest reduction in EMG amplitude. As for the mechanism, we suggest that US waves stretched the axonal ion channels and modified the gating kinetics which in return changed the propagation of the action potential and hence the release of ACh moles at the neuromuscular junction. Testing this hypothesis requires injecting specific channel blockers while treating the nerve with US.

Another future work is to explore the effect of baseline activity of the nerve on its response to US stimulation: sonication parameters are kept the same, but the input electrical stimulus pre-sonication is altered across trials.

It will finally be beneficial to undergo the experiment non-invasively where the transducer is positioned on the shaved skin and targeting the sciatic nerve using US-guided imaging.

APPENDIX

A. Calculation of Acoustic Intensity

The acoustic intensity of ultrasonic waves was computed from the acquired voltage measurements in the following steps according to the Food and Drug Administration (2019).

First, the pulse intensity integral (PII) was computed, defined as the time integral of instantaneous intensity integrated over the time in which the hydrophone signal for the specific pulse is nonzero. The instantaneous acoustic intensity i is

$$\text{expressed as: } i = \frac{p^2}{\rho * c}$$

Where p is the acoustic pressure, ρ is the density of medium (water in this case), and c the speed of sound in medium.

$$\text{The pressure } p \text{ is expressed as } p(t) = \frac{v(t)}{M}$$

Where $v(t)$ is the acquired voltage array that varies with the position of hydrophone with respect to transducer, and M is the overall sensitivity expressed as $M = M_{EOC} * \frac{C_h}{C_h + C_{cable} + C_{scope}}$

$$\frac{C_h}{C_h + C_{cable} + C_{scope}}$$

Where M_{EOC} is the end-of-cable (EOC) nominal sensitivity of hydrophone, C_h the capacitance of the hydrophone, C_{cable} the capacitance of the extension cable between the hydrophone and oscilloscope, and C_{scope} the input capacitance of the oscilloscope.

Hence, PII is expressed as:

$$PII = \frac{\int_{t_1}^{t_2} p^2(t) dt}{\rho * c} = \frac{\int_{t_1}^{t_2} v^2(t) dt}{\rho * c * M^2}$$

where $(t_2 - t_1)$ is the interval in which the amplitude of the recorded voltage is nonzero (i.e. $t_2 - t_1 = \text{tone-burst-duration or TBD}$).

PII corresponds to the energy transferred per unit area (expressed in J/m²) or the energy fluence during one pulse.

Then, the pulse duration (PD) was calculated, defined as:

$$PD = 1.25 * (t_4 - t_3)$$

where t_4 is the time instant at which the time integral of intensity reaches 90 percent of PII, and t_3 is the instant at which the time integral reaches 10 percent of PII.

Finally, the spatial-peak pulse-average intensity (I_{SPPA}) was calculated as the maximum ratio of PII (energy fluence per pulse) to PD.

$$I_{SPPA} = \frac{PII}{PD}$$

B. Properties of devices used in experiments of Chapter III

In experiments that explore the change of acoustic intensity with respect to experimental parameters, we used a 2-channel Siglent Arbitrary Waveform Generator (SDG 2042X; maximum output = 40MHz; maximum sampling rate = 1.2GSa/s; 50 Ω impedance) and RF power amplifier from Electronics and Innovation (model number 2100L; 1.0 V_{rms} input; 50 Ω input/output impedance).

Table 6 provides the properties of the focused transducers that were used. All the transducers are from Olympus and have an outer diameter of 25.4 mm. The users shall not submerge the transducer for periods exceeding 8 hours and must allow 16 hours of dry time to ensure the life of the unit.

Table 5: Properties of Olympus focused transducers used in the experiments of Chapter III

Serial number	Frequency (MHz)	Focal length (mm)	Center frequency (MHz)	Peak frequency (MHz)	(-6) dB bandwidth (%)
1252324	1.00	37.19	0.96	1.04	73.35
1251995	5.00	39.52	4.77	4.86	66.52
1251991	7.50	36.4	6.76	7.26	83.95

The oscilloscope channel of the data-acquisition board (National Instruments Elvis III) has an input capacitance of 15 pF, which was accounted in the calculation of the overall sensitivity. Also, the oscilloscope channel requires an input voltage that does not exceed 50 volts direct current, or 30 volts root mean square (RMS) for alternating current. When visualizing the voltage, the oscilloscope can measure a range of 2 volts peak-to-peak for a display less or equal to than 200 mV per division, and a range of 50 volts peak-to-peak for a display greater than 200 mV per division.

The Sonic Concepts Y-104-023 hydrophone, used in experiments of subsection B.3. of chapter III, has an operating frequency range of 0.050 to 1.90 MHz, a maximum operating temperature of 50 °C, a frequency-dependent sensitivity, and a frequency-dependent capacitance, provided in table 7.

Table 6: EOC sensitivity and capacitance of the Sonic Concepts Y-104-023 hydrophone used in experiments of subsection B.3. of Chapter III

Frequency (MHz)	EOC Sensitivity (dB Re 1V/μPa)	EOC Sensitivity (V/MPa)	Capacitance (pF)	Overall sensitivity (V/MPa)
0.50	-209.3	34.874	155.27	31.802
0.80	-211.3	27.227	155.5	24.832
1.00	-212.6	23.442	151.6	21.332
1.20	-213.8	20.417	142.7	18.475

The Onda HNR-0500 hydrophone, used in experiments subsection B.1, B.2, and B.4 of chapter III, has an operating frequency range of 0.25 to 10 MHz, a maximum operating temperature of 50 °C, a capacitance of 200 pF, and a frequency-dependent sensitivity, provided in table 8.

The hydrophones were attached to a motorized axis system from Velmex consisting of three motors (VXM-3).

Table 7: EOC sensitivity and capacitance of the Onda HNR-0500 hydrophone used in experiments of subsection B.1, B.2, and B.4 of Chapter III

Frequency (MHz)	EOC Sensitivity (dB Re 1V/μPa)	EOC Sensitivity (V/MPa)	Capacitance (pF)	Overall sensitivity (V/MPa)
0.50	-255	0.178	200	0.165
0.80	-257	0.141	200	0.131
1.00	-258	0.126	200	0.117
1.20	-261	0.089	200	0.083
5.00	-256.5	0.150	200	0.139
7.5	-256.2	0.155	200	0.144

C. Full-width colormaps

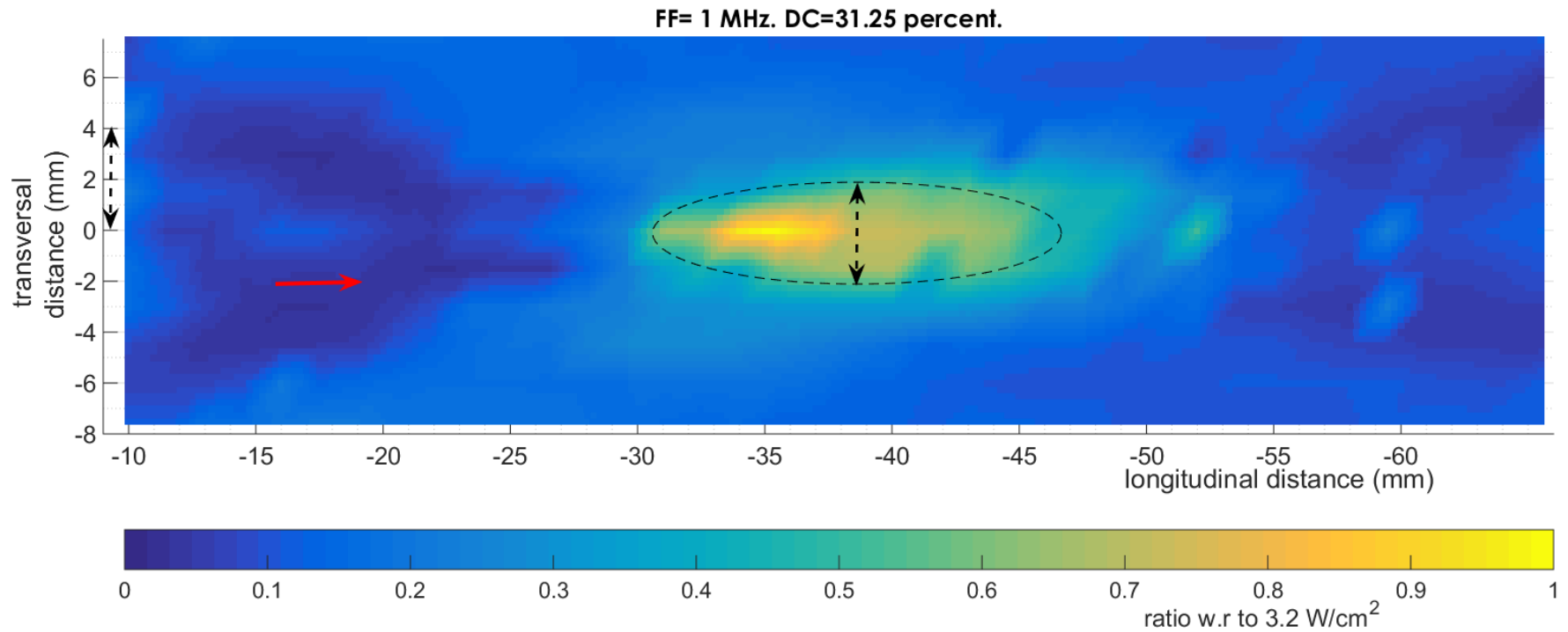


Figure 30: Colormap of normalized spatial-peak pulse average intensity (I_{SPPA}) at FF= 1 MHz. DC= 31.25 percent. The black double arrow represents the diameter of the focus measured at FWHM (4 mm). The red arrow indicates the direction of US. (Parameters: FF= 1 MHz. CPP=250. BP= 800 μ s. Amplitude of generated signal= 225 mVpp.)

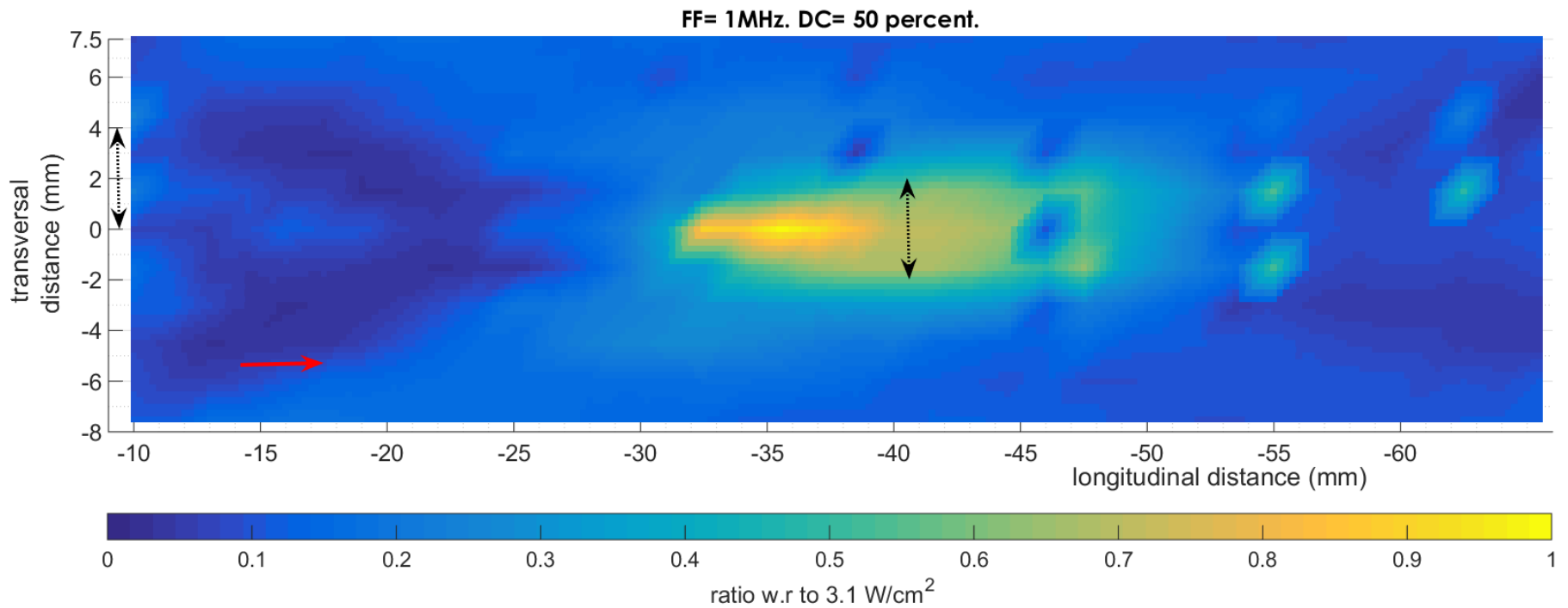


Figure 31: Colormap of normalized spatial-peak pulse average intensity (I_{SPPA}) at FF= 1 MHz. DC= 50 percent. The black double arrow represents the diameter of the focus measured at FWHM (4 mm). The red arrow indicates the direction of US. (Parameters: FF= 1 MHz. CPP=250. BP= 500 μs . Amplitude of generated signal= 225 mVpp.)

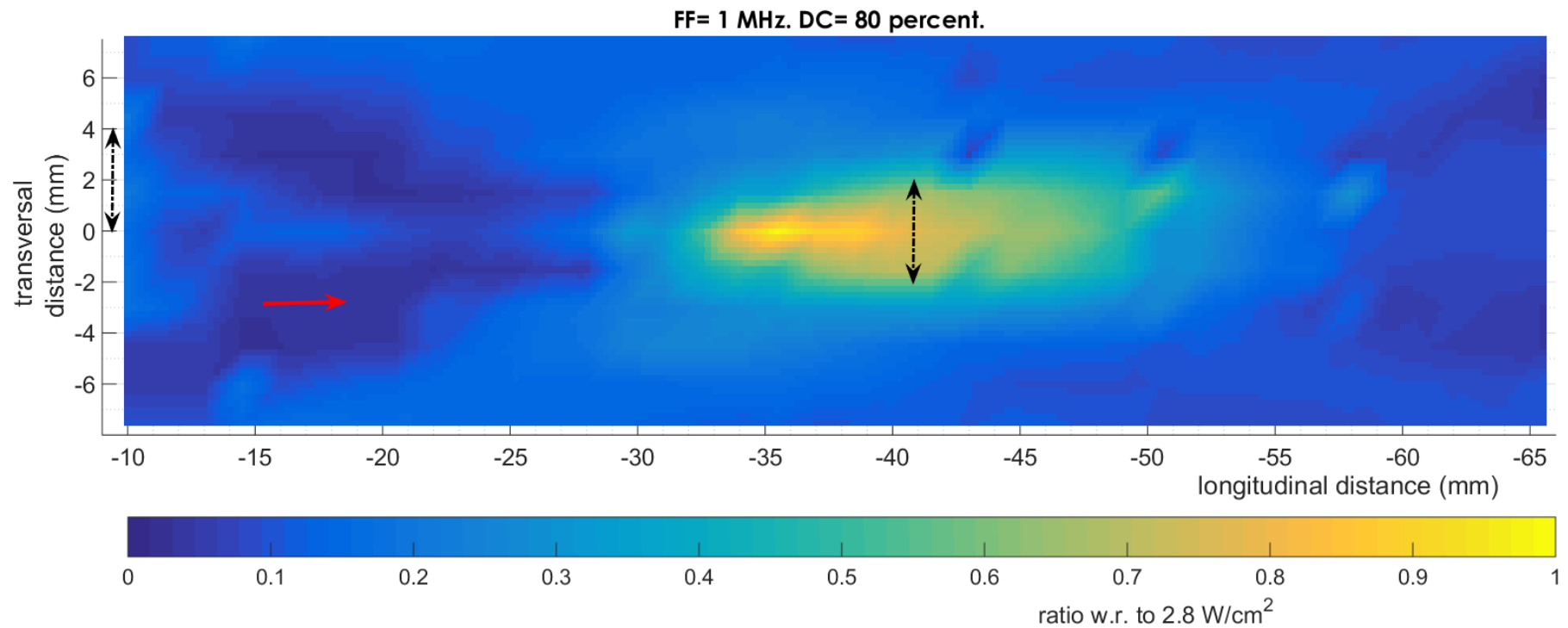


Figure 32: Colormap of normalized spatial-peak pulse average intensity (I_{SPPA}) at FF= 1 MHz. DC= 31.25 percent. The black double arrow represents the diameter of the focus measured at FWHM (4 mm). The red arrow indicates the direction of US. (Parameters: FF= 1 MHz. CPP=250. BP= 312.5 μs . Amplitude of generated signal= 225 mVpp.)

D. Preparation of the gelatin-based phantom (section B.3 of Chapter II)

We prepared the gelatin-based tissue mimicking phantom using the recipe of Dahmani et al. (2019):

Step 0: Measure the mass of gelatin powder required to achieve the desired concentration.

Step 1: Heat osmosed water using a hot plate until the water temperature reaches 60 °C. Turn off the heat source when reaching this temperature.

Step 2: Slowly sprinkle the gelatin powder in hot water and stir using a magnetic stirrer.

Step 3: Once the powder dissolves, remove air bubbles using a spatula.

Step 4: Pour the mixture in a mold and place the mold in a conventional household refrigerator for 24 hours.

E. Time plots of amplitude and AUC for each trial (experiments of chapter IV)

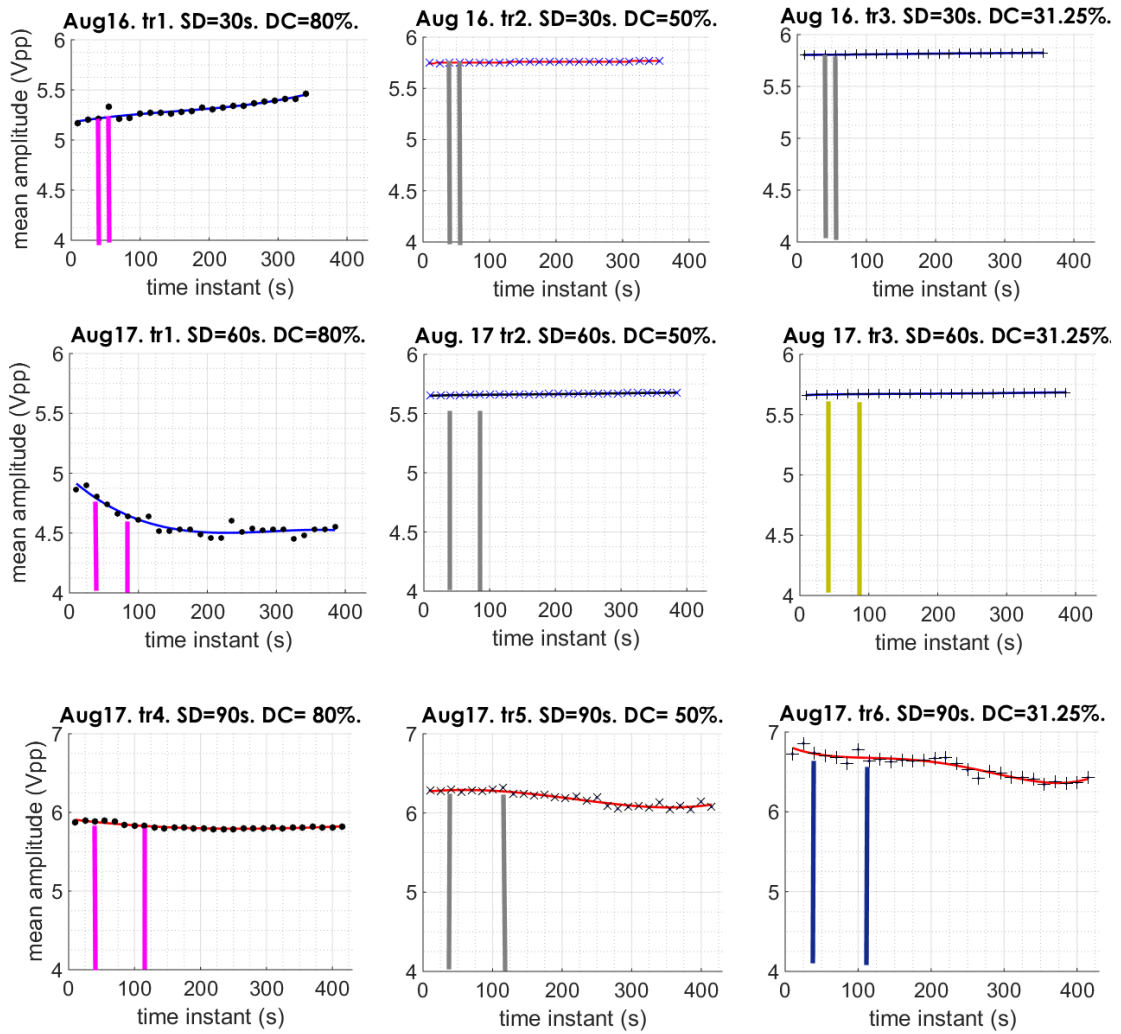


Figure 33: Trials of August 16 and 17. Mean amplitude with a polynomial fit. The bars correspond to start and end of sonication session.

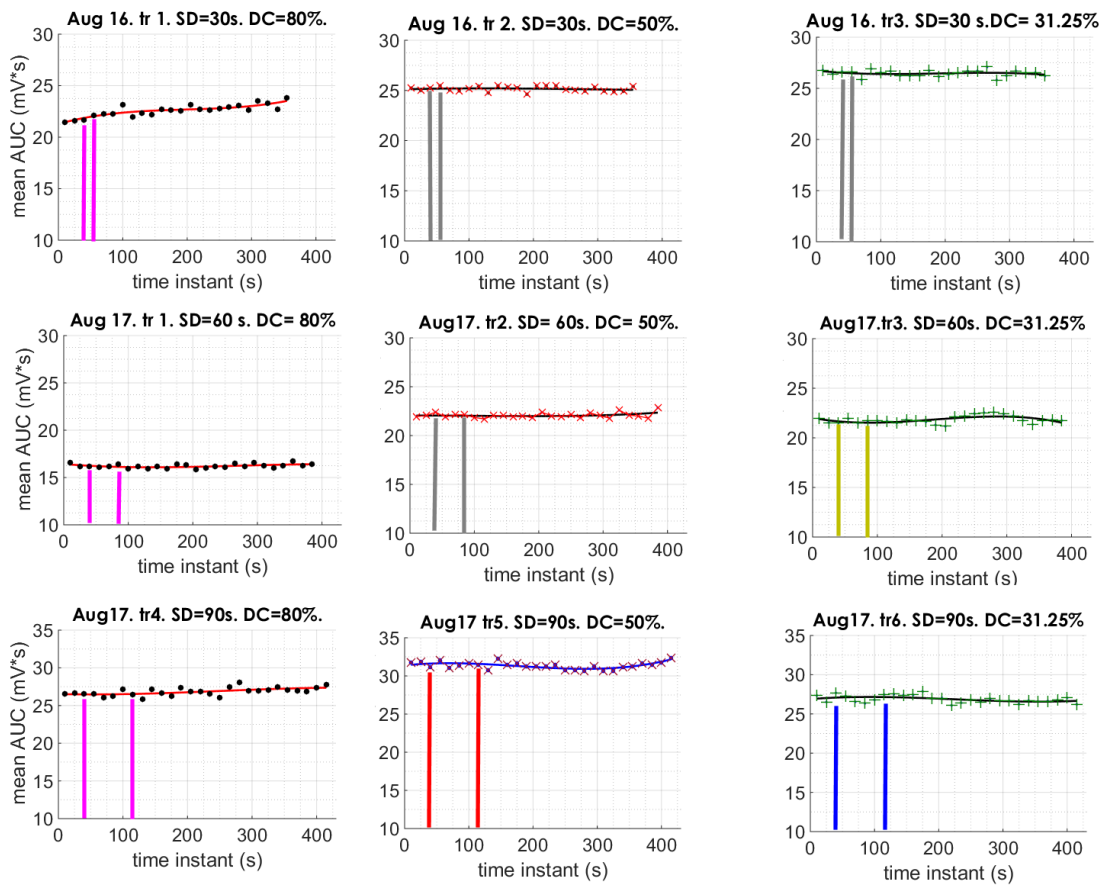


Figure 34: Trials of August 16 and 17. Mean AUC computed for each 15-second interval in each trial along with a polynomial fit. The bars correspond to start and end of sonication session.

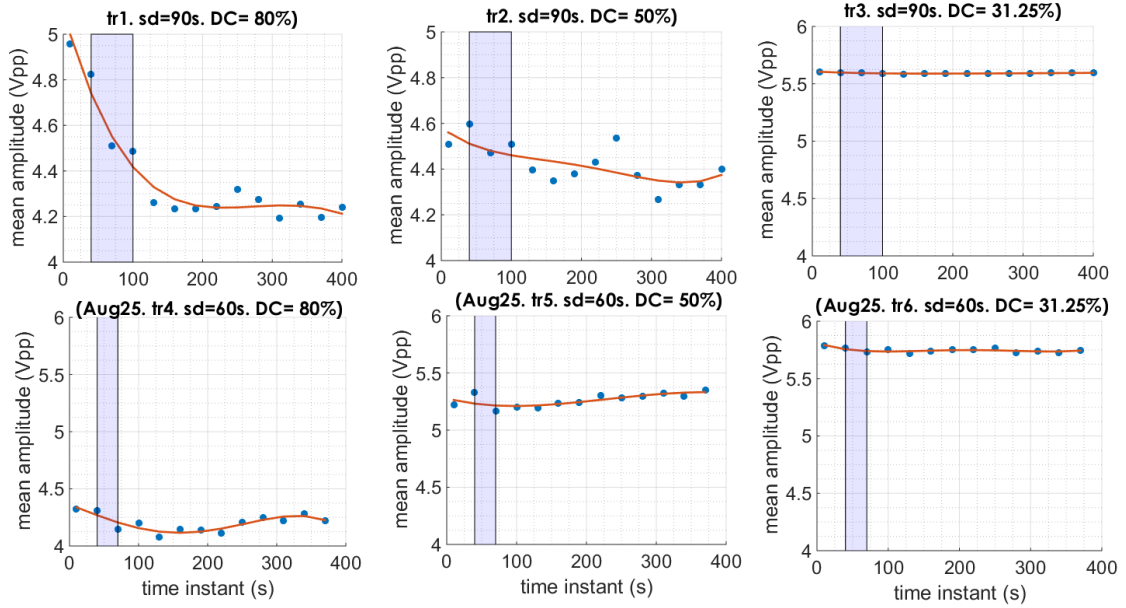


Figure 35: Trials of August 25. Mean amplitude with a polynomial fit. The shaded area represents sonication session. The points on the limits of the shaded area belong to the area.

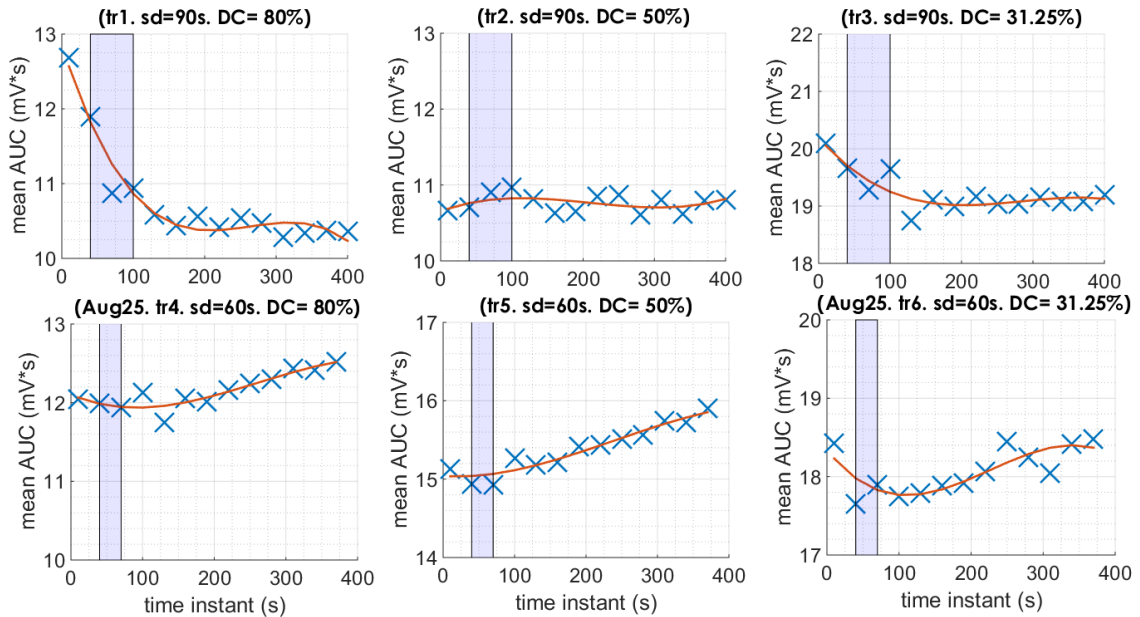


Figure 36: Trials of August 25. Mean AUC with a polynomial fit. The shaded area represents sonication session. The points on the limits of the shaded area belong to the area.

F. The processes that lead to movement of skeletal muscle

Triggering muscle fibers starts with an impulse in the motor nerve (Luzi, 2012, p. 13-14). The action potential propagates from the motor neuron down to the axon by

the activation of the sodium and potassium channels. The arrival of the action potential to the presynaptic end leads to an influx of calcium ions; the influx causes the vesicles that contain acetylcholine (ACh) to fuse with the plasma membrane and release the neurotransmitter into the extracellular space between the neuron and the muscle cell. ACh binds to its receptors on the motor end plate of the muscle cells. The activation of the receptors triggers a series of events whose end result is muscle movement.

G. Structures of ion channels

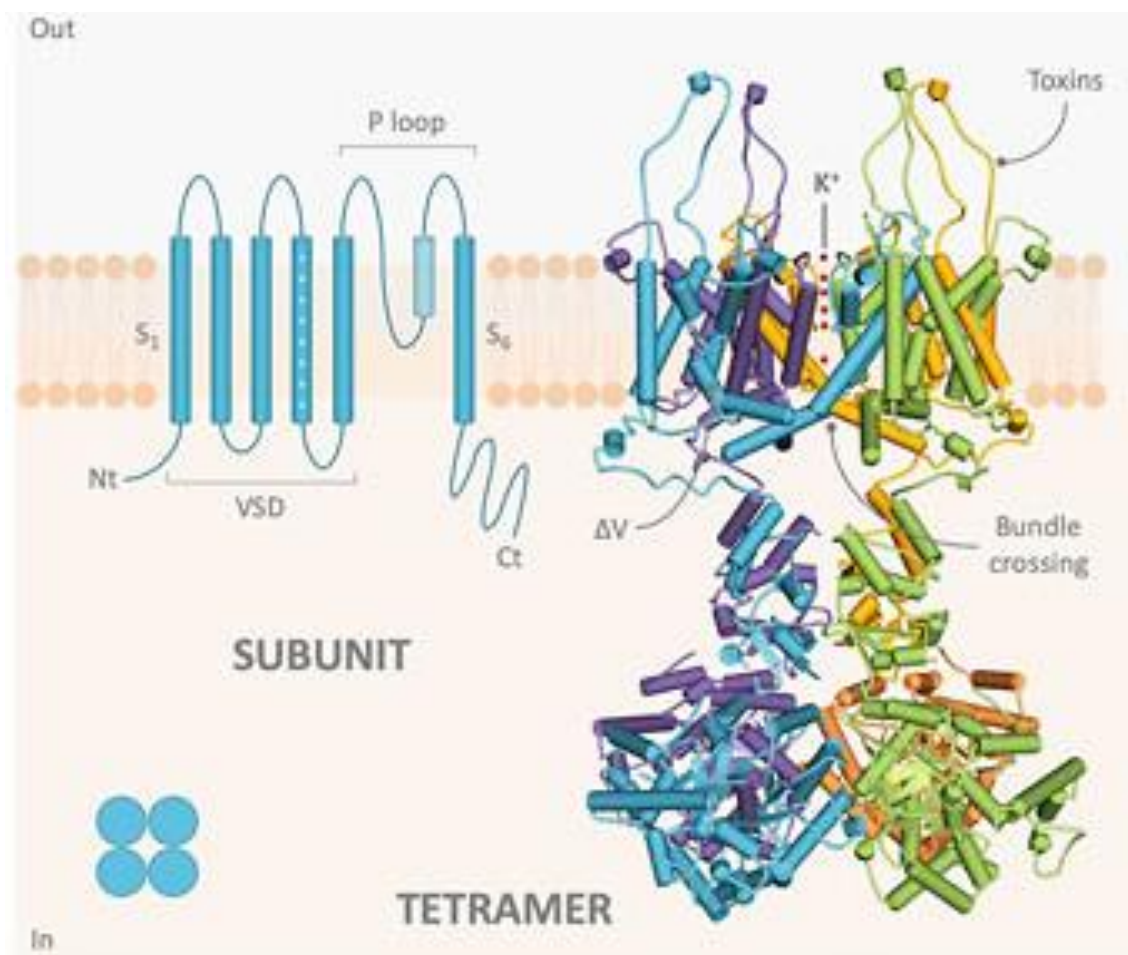


Figure 37: structure of the VGKCs of the Kv subfamily (Gamper & Wang, 2021, p. 6). The channel has a voltage-sensing domain (VSD) that detects voltage difference during firing, and a pore domain through which potassium ions diffuse.

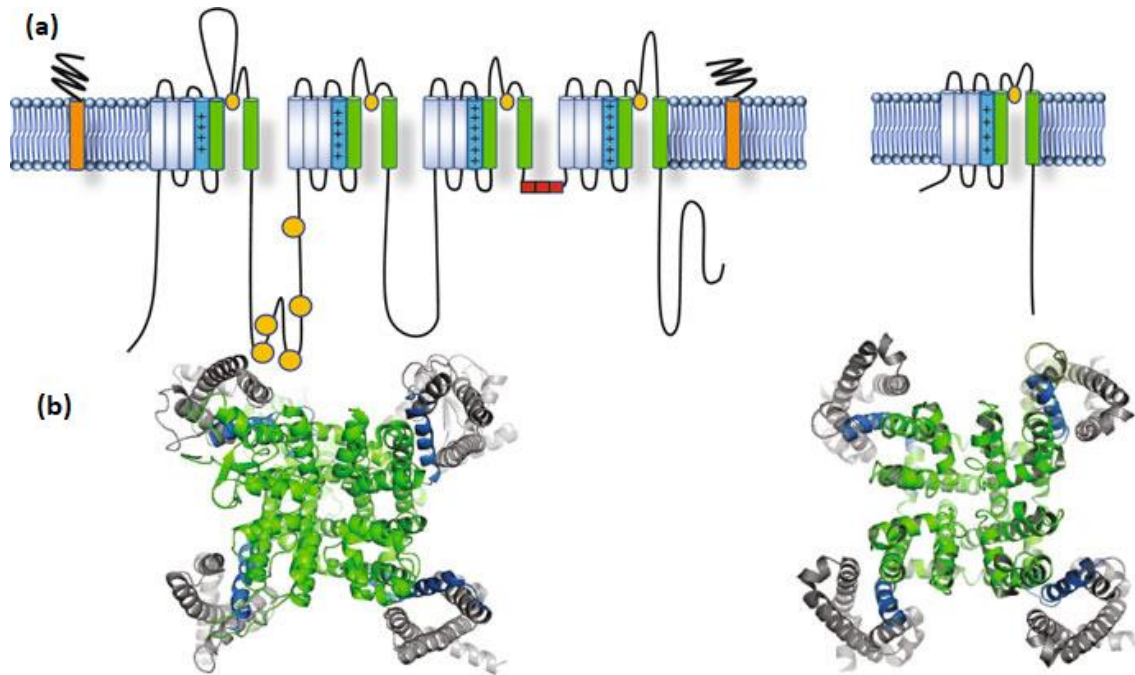


Figure 38: (a) schematic of overall structure of voltage-gated sodium channel (Nav), having a VSD, and a pore domain. (b) Top view of overall model of eukaryotic (left) and bacterial (right) voltage-gated sodium channel (Chahine, 2018, p.55).

REFERENCES

- Ambrosino, P., Soldovieri, M. V., Di Zazzo, E., Paventi, G., Iannotti, F. A., Mosca, I., ... & Taglialatela, M. (2019). Activation of Kv7 potassium channels inhibits intracellular Ca²⁺ increases triggered by TRPV1-mediated pain-inducing stimuli in F11 immortalized sensory neurons. *International Journal of Molecular Sciences*, 20(18), 4322.
- Azhari, H. (2010). *Basics of biomedical ultrasound for engineers*. John Wiley & Sons.
- Blackmore, J., Shrivastava, S., Sallet, J., Butler, C. R., & Cleveland, R. O. (2019). Ultrasound neuromodulation: a review of results, mechanisms and safety. *Ultrasound in medicine & biology*, 45(7), 1509-1536.
- Bobola, M. S., Chen, L., Ezeokeke, C. K., Kuznetsova, K., Lahti, A. C., Lou, W., ... & Mourad, P. D. (2018). A review of recent advances in ultrasound, placed in the context of pain diagnosis and treatment. *Current pain and headache reports*, 22(9), 1-13.
- Centers for Disease Control and Prevention (CDC) (2012). CDC grand rounds: prescription drug overdoses-a US epidemic. *MMWR. Morbidity and mortality weekly report*, 61(1), 10-13.
- Chahine, M. (2018). *Voltage-gated sodium channels: structure, function and channelopathies*. Cham: Springer International Publishing.
- Chen, R. J., Lin, C. C. K., & Ju, M. S. (2010a). In situ transverse elasticity and blood perfusion change of sciatic nerves in normal and diabetic rats. *Clinical Biomechanics*, 25(5), 409-414.

- Chen, R. J., Lin, C. C. K., & Ju, M. S. (2010b). In situ biomechanical properties of normal and diabetic nerves: an efficient quasi-linear viscoelastic approach. *Journal of biomechanics*, *43*(6), 1118-1124.
- Chen, A. I., Balter, M. L., Chen, M. I., Gross, D., Alam, S. K., Maguire, T. J., & Yarmush, M. L. (2016). Multilayered tissue mimicking skin and vessel phantoms with tunable mechanical, optical, and acoustic properties. *Medical physics*, *43*(6Part1), 3117-3131.
- Clennell, B., Steward, T. G., Elley, M., Shin, E., Weston, M., Drinkwater, B. W., & Whitcomb, D. J. (2021). Transient ultrasound stimulation has lasting effects on neuronal excitability. *Brain Stimulation*, *14*(2), 217-225.
- Coutinho, A. B. B., Jotta, B., Werneck-de-Castro, J. P., Pino, A. V., & Souza, M. N. (2020). Invasive electrical impedance myography at different levels of contraction of gastrocnemius muscle of rat. *Review of Scientific Instruments*, *91*(8), 084103.
- Culjat, M. O., Goldenberg, D., Tewari, P., & Singh, R. S. (2010). A review of tissue substitutes for ultrasound imaging. *Ultrasound in medicine & biology*, *36*(6), 861-873.
- da Silva Freitas, T., de Monaco, B. A., & Golovac, S. (2022). *Neuromodulation Techniques for Pain Treatment: A Step-By-Step Guide to Interventional Procedures and Managing Complications*. Springer International Publishing AG.
- Dahmani, J., Laporte, C., Pereira, D., Bélanger, P., & Petit, Y. (2019). Predictive model for designing soft-tissue mimicking ultrasound phantoms with adjustable

- elasticity. *IEEE Transactions on Ultrasonics, Ferroelectrics, and Frequency Control*, 67(4), 715-726.
- Deardorff, A. S., Romer, S. H., & Fyffe, R. E. (2021). Location, location, location: the organization and roles of potassium channels in mammalian motoneurons. *The Journal of Physiology*, 599(5), 1391-1420.
- Dedola, F., Severino, F. P. U., Meneghetti, N., Lemaire, T., Cafarelli, A., Ricotti, L., ... & Micera, S. (2020). Ultrasound stimulations induce prolonged depolarization and fast action potentials in leech neurons. *IEEE open journal of engineering in medicine and biology*, 1, 23-32.
- Dell'Italia, J., Sanguinetti, J. L., Monti, M. M., Bystritsky, A., & Reggente, N. (2022). Current State of Potential Mechanisms Supporting Low Intensity Focused Ultrasound for Neuromodulation. *Frontiers in Human Neuroscience*, 16.
- Drost, L., Hynynen, K., Huang, Y., Lucht, B., Wong, E., Czarnota, G., Yee, C., Wan, B. A., Ganesh, V., Chow, E., & David, E. (2020). Ultrasound-Guided Focused Ultrasound Treatment for Painful Bone Metastases: A Pilot Study. *Ultrasound in Medicine & Biology*.
- El Hassan, R. H. (2020). *Low intensity ultrasound for suppression of peripheral nerve activity* [unpublished master's thesis]. American University of Beirut.
- Food and Drug Administration. (2019). Marketing clearance of diagnostic ultrasound systems and transducers.
- Fomenko, A., Chen, K. H. S., Nankoo, J. F., Saravanamuttu, J., Wang, Y., El-Baba, M., ... & Chen, R. (2020). Systematic examination of low-intensity ultrasound parameters on human motor cortex excitability and behavior. *Elife*, 9, e54497.

- Freije, A. S. (2022). *Ablation of 3D cancer tumor spheroids using High Intensity Focused Ultrasound (HIFU)* [unpublished master's thesis]. American University of Beirut.
- Gallay, M. N., Moser, D., & Jeanmonod, D. (2020). MR-guided focused ultrasound central lateral thalamotomy for trigeminal neuralgia. Single center experience. *Frontiers in Neurology, 11*, 271.
- Gamper, N., & Wang, K. (2021). *Pharmacology of Potassium Channels* (Vol. 267). Springer Nature.
- Grubb, M. S., Shu, Y., Kuba, H., Rasband, M. N., Wimmer, V. C., & Bender, K. J. (2011). Short-and long-term plasticity at the axon initial segment. *Journal of Neuroscience, 31*(45), 16049-16055.
- Guimarães, C. F., Gasperini, L., Marques, A. P., & Reis, R. L. (2020). The stiffness of living tissues and its implications for tissue engineering. *Nature Reviews Materials, 5*(5), 351-370.
- Hargreaves, M., & Spriet, L. L. (2006). *Exercise metabolism*. Human kinetics.
- Hellman, A., Clum, A., Maietta, T., Srikanthan, A., Patel, V., Panse, D., ... & Pilitsis, J. G. (2021). Effects of external low intensity focused ultrasound on inflammatory markers in neuropathic pain. *Neuroscience Letters, 757*, 135977.
- Jacquet, E., Chambert, J., Pauchot, J., & Sandoz, P. (2017). Intra-and inter-individual variability in the mechanical properties of the human skin from in vivo measurements on 20 volunteers. *Skin Research and Technology, 23*(4), 491-499.
- Joe, H., Pahk, K. J., Park, S., & Kim, H. (2019). Development of a subject-specific guide system for Low-Intensity Focused Ultrasound (LIFU) brain stimulation. *Computer methods and programs in biomedicine, 176*, 105-110.

- Kalso, E., Edwards, J. E., Moore, R. A., & McQuay, H. J. (2004). Opioids in chronic non-cancer pain: systematic review of efficacy and safety. *Pain, 112*(3), 372-380.
- Kohno, T., Ji, R. R., Ito, N., Allchorne, A. J., Befort, K., Karchewski, L. A., & Woolf, C. J. (2005). Peripheral axonal injury results in reduced μ opioid receptor pre- and post-synaptic action in the spinal cord. *Pain, 117*(1-2), 77-87.
- Krasovitski, B., Frenkel, V., Shoham, S., & Kimmel, E. (2011). Intramembrane cavitation as a unifying mechanism for ultrasound-induced bioeffects. *Proceedings of the National Academy of Sciences, 108*(8), 3258-3263.
- Kubanek, J., Shi, J., Marsh, J., Chen, D., Deng, C., & Cui, J. (2016). Ultrasound modulates ion channel currents. *Scientific reports, 6*(1), 1-14.
- Kurdi, A. (2021). Opioids and Gabapentinoids Utilisation and Their Related-Mortality Trends in the United Kingdom Primary Care Setting, 2010–2019: A Cross-National, Population-Based Comparison Study. *Frontiers in Pharmacology, 12*.
- Liang, D., Chen, J., Zhou, W., Chen, J., Chen, W., & Wang, Y. (2020). Alleviation Effects and Mechanisms of Low-intensity Focused Ultrasound on Pain Triggered by Soft Tissue Injury. *Journal of Ultrasound in Medicine, 39*(5), 997-1005.
- Liu, Y., Wang, G., Cao, C., Zhang, G., Tanzi, E. B., Zhang, Y., ... & Li, Y. (2021). Neuromodulation effect of very low intensity transcranial ultrasound stimulation on multiple nuclei in rat brain. *Frontiers in Aging Neuroscience, 13*, 656430.
- Lin, Z., Meng, L., Zou, J., Zhou, W., Huang, X., Xue, S., ... & Zheng, H. (2020). Non-invasive ultrasonic neuromodulation of neuronal excitability for treatment of epilepsy. *Theranostics, 10*(12), 5514.

- Luzi, L. (2012). *Cellular physiology and metabolism of physical exercise*. Springer.
- Maccabi, A., Shin, A., Namiri, N. K., Bajwa, N., St. John, M., Taylor, Z. D., ... & Saddik, G. N. (2018). Quantitative characterization of viscoelastic behavior in tissue-mimicking phantoms and ex vivo animal tissues. *PloS one*, *13*(1), e0191919.
- McArdle, W. D., Katch, F. I., & Katch, V. L. (2001). *Exercise physiology: energy, nutrition, and human performance*. Lippincott Williams & Wilkins, Philadelphia.
- McCrum, N. G., Buckley, C. P., Buckley, C. P., & Bucknall, C. B. (2001). *Principles of polymer engineering*. Oxford University Press, USA.
- Morris, C. E., & Juranka, P. F. (2007). Nav channel mechanosensitivity: activation and inactivation accelerate reversibly with stretch. *Biophysical journal*, *93*(3), 822-833.
- Naeije, M., & Zorn, H. (1982). Relation between EMG power spectrum shifts and muscle fibre action potential conduction velocity changes during local muscular fatigue in man. *European journal of applied physiology and occupational physiology*, *50*(1), 23-33.
- Naor, O., Krupa, S., & Shoham, S. (2016). Ultrasonic neuromodulation. *Journal of neural engineering*, *13*(3), 031003.
- Niu, X., Yu, K., & He, B. (2022). Transcranial focused ultrasound induces sustained synaptic plasticity in rat hippocampus. *Brain Stimulation*, *15*(2), 352-359.
- Nguyen, J. P., Lefaucheur, J. P., Decq, P., Uchiyama, T., Carpentier, A., Fontaine, D., ... & Keravel, Y. (1999). Chronic motor cortex stimulation in the treatment of

central and neuropathic pain. Correlations between clinical, electrophysiological and anatomical data. *Pain*, 82(3), 245-251.

Nguyen, D. T., Berisha, D. E., Konofagou, E. E., & Dmochowski, J. P. (2022).

Neuronal responses to focused ultrasound are gated by pre-stimulation brain rhythms. *Brain Stimulation*, 15(1), 233-243.

Palacio-Torralba, J., Hammer, S., Good, D. W., McNeill, S. A., Stewart, G. D., Reuben, R. L., & Chen, Y. (2015). Quantitative diagnostics of soft tissue through viscoelastic characterization using time-based instrumented palpation. *Journal of the mechanical behavior of biomedical materials*, 41, 149-160.

Plaksin, M., Kimmel, E., & Shoham, S. (2016). Cell-type-selective effects of intramembrane cavitation as a unifying theoretical framework for ultrasonic neuromodulation. *Eneuro*, 3(3).

Priori, A., Berardelli, A., Rona, S., Accornero, N., & Manfredi, M. (1998). Polarization of the human motor cortex through the scalp. *Neuroreport*, 9(10), 2257-2260.

Roux, F. E., Ibarrola, D., Lazorthes, Y., & Berry, I. (2001). Chronic motor cortex stimulation for phantom limb pain: a functional magnetic resonance imaging study: technical case report. *Neurosurgery*, 48(3), 681-688.

Rubiano, A., Delitto, D., Han, S., Gerber, M., Galitz, C., Trevino, J., ... & Simmons, C. S. (2018). Viscoelastic properties of human pancreatic tumors and in vitro constructs to mimic mechanical properties. *Acta biomaterialia*, 67, 331-340.

Safa, B. N., Read, A. T., & Ethier, C. R. (2021). Assessment of the viscoelastic mechanical properties of the porcine optic nerve head using micromechanical testing and finite element modeling. *Acta Biomaterialia*, 134, 379-387.

- Shamji, M. F., De Vos, C., & Sharan, A. (2017). The advancing role of neuromodulation for the management of chronic treatment-refractory pain. *Neurosurgery*, *80*(3S), S108-S113.
- Singh, S. P., William, M., Malavia, M., & Chu, X. P. (2022). Behavior of KCNQ Channels in Neural Plasticity and Motor Disorders. *Membranes*, *12*(5), 499.
- Tanei, T., Kajita, Y., & Wakabayashi, T. (2010). Motor Cortex Stimulation for Intractable Neuropathic Facial Pain Related to Multiple Sclerosis—Case Report—. *Neurologia medico-chirurgica*, *50*(7), 604-607.
- Todd, N., McDannold, N., & Borsook, D. (2020). Targeted manipulation of pain neural networks: The potential of focused ultrasound for treatment of chronic pain. *Neuroscience & Biobehavioral Reviews*.
- Vasu, S. O., & Kaphzan, H. (2021). The role of sodium channels in direct current stimulation—axonal perspective. *Cell Reports*, *37*(2), 109832.
- Vasu, S. O., & Kaphzan, H. (2022). The role of axonal voltage-gated potassium channels in tDCS. *Brain Stimulation*, *15*(3), 861-869.
- Vatanpour, H., & Harvey, A. L. (1995). Modulation of acetylcholine release at mouse neuromuscular junctions by interaction of three homologous scorpion toxins with K⁺ channels. *British journal of pharmacology*, *114*(7), 1502-1506.
- Wang, X., Burke, S. R., Talmadge, R. J., Voss, A. A., & Rich, M. M. (2020). Depressed neuromuscular transmission causes weakness in mice lacking BK potassium channels. *Journal of General Physiology*, *152*(5).
- Wong, Y.-C. (2005) *Biomechanical Properties of Rat Sciatic Nerve*, [master's thesis]. Central University, Chung-Li, Taiwan.

- Yazdi, S. J. M., & Baqersad, J. (2022). Mechanical modeling and characterization of human skin: A review. *Journal of Biomechanics*, *130*, 110864.
- Yoo, S. S., Yoon, K., Croce, P., Cammalleri, A., Margolin, R. W., & Lee, W. (2018). Focused ultrasound brain stimulation to anesthetized rats induces long-term changes in somatosensory evoked potentials. *International journal of imaging systems and technology*, *28*(2), 106-112.
- Yoo, S., Mittelstein, D. R., Hurt, R. C., Lacroix, J., & Shapiro, M. G. (2022). Focused ultrasound excites cortical neurons via mechanosensitive calcium accumulation and ion channel amplification. *Nature communications*, *13*(1), 1-13.
- Yu, K., Niu, X., & He, B. (2020). Neuromodulation Management of Chronic Neuropathic Pain in the Central Nervous System. *Advanced Functional Materials*, *30*(37), 1908999.
- Zhang, M., Rodrigues, A., Zhou, Q., & Li, G. (2022). Focused ultrasound: growth potential and future directions in neurosurgery. *Journal of neuro-oncology*, *156*(1), 23–32.
- Zhang, S., Kang, M., Xu, Y., Li, C., & Dong, F. (2022). Finite-Element Modeling of Tissue Responses to Focused Ultrasound With Different Intensities. *IEEE Transactions on Instrumentation and Measurement*, *71*, 1-10.
- Zou, J., Meng, L., Lin, Z., Qiao, Y., Tie, C., Wang, Y., ... & Zheng, H. (2020). Ultrasound neuromodulation inhibits seizures in acute epileptic monkeys. *Iscience*, *23*(5), 10106